(ISSN NO. (Print) : 2347-6982, (Online): 2349-204X)

International Journal of Industrial Electronics and Electrical Engineering

Volume No. 12
Issue No. 1
January - April 20244

ENRICHED PUBLICATIONS PVT. LTD

S-9, IInd FLOOR, MLU POCKET,
MANISH ABHINAV PLAZA-II, ABOVE FEDERAL BANK,
PLOT NO-5, SECTOR-5, DWARKA, NEW DELHI, INDIA-110075,
PHONE: - + (91)-(11)-47026006

(ISSN NO. (Print) : 2347-6982, (Online): 2349-204X)

International Journal of Industrial Electronics and Electrical Engineering

Aim & Scope

"International Journal of Industrial Electronics and Electrical Engineering (IJIEEE)" (ISSN NO. (Print) : 2347-6982, (Online): 2349-204X) a peer-reviewed and free open access journal aim to provide the complete and a reliable source of information on current developments in the fields of Electronics and Electrical Engineering. The emphasis will be on publishing quality articles rapidly and openly available to researchers worldwide.

Manuscripts submitted to **"International Journal of Industrial Electronics and Electrical Engineering (IJIEEE)"** must be prepared in English and are subject to a rigorous and fair peer-review process. All submitted papers must be original work that has not been published or under consideration for publication elsewhere. Manuscripts should be typed double space on A4 size paper using font size 12 and preferably not more than 8 pages in length inclusive of tables, figures and illustrations.

All submissions will be peer-reviewed. The scope of **"International Journal of Industrial Electronics and Electrical Engineering (IJIEEE)"** covers all aspects of Electrical, Electronics, Instrumentation, Industrial Electronics, and Communication Technology etc.

(ISSN NO. (Print) : 2347-6982, (Online): 2349-204X)

Editor-in-Chief

(ISSN NO. (Print) : 2347-6982, (Online): 2349-204X)

(ISSN NO. (Print) : 2347-6982, (Online): 2349-204X)

International Journal of Industrial Electronics and Electrical Engineering (IJIEEE)

(Volume No. 12, Issue No. 1, January - April 2024)

Contents

(ISSN NO. (Print) : 2347-6982, (Online): 2349-204X)

A Cry Detection Method in Real Neonatal Intensive Care Units

[1]Manh Chinh Dang, [2]Huy Hoang Vuong, [3]Thi Quyen Vu, [4]Duy Khanh Nguyen, [5]Thanh Trung Dang

[1,2,3] Researcher, Institue of Information Technology, 18 Hoang Quoc Viet Road, Hanoi
[4]Student, Hanoi University of Industry, 298 Cau Dien Road, Hanoi 5Lecturer, Electric Power University,
[235] Hoang Quoc Viet Road, Hanoi
E-mail: [1]dangmanhchinhbkhn@gmail.com, [2]hoangtdhk54@gmail.com, [3]vtquyen@ioit.ac.vn, [4]tonykhanh1103@gmail.com, [5]thanhtrungepu@gmail.com

A B S T R A C T

The cry detection is very important in intelligent computerized systems to evaluate the wellbeing of neonates during their hospitalization periods. In addition, cry's classification provides useful information (eg: tiredness, pain, hunger, ...). Although several cry detection and characterization techniques can be found in the literature, the testing in real-life environments such as hospital Intensive Care Units is limited. In this article, first, we revise the background noise in Intensive Care Units,that may affect the cry detection algorithms' result. Second, we implement a specific cry detection technique that is based on deep learning. Finally, we assess this method using audio samples recorded in a real neonatal intensive care unit and compare result to previous method of frequency different.

Keywords - Deep Learning, Neural Network, Cry detection, Fundamental Frequency.

I. INTRODUCTION

Some newborns have to spend a period of time in Neonatal Intensive Care Units (NICUs). Most of them are preterm newborns who suffer from some immaturity or disease. During hospitalization, newborns might suffer from pain (for instance, due to invasive procedures) and if this pain is not treated correctly, the child could suffer from some neurological disorders in the future. In order to detect whether neonatal patients are suffering from pain or discomfort, health professionals proceed by directly observing physiological parameters (i.e. heartbeat rate, temperature, etc.) and behavioral parameters (frowning, crying…) and using some assessment scales to figure out if some pain must be relieved. These procedures are done in an hourly basis, by a reduced number of people that also take care of the other typical duties in the NICUs.

Moreover, current trends in nursing for the neonates focus on personalized observations of the newborn (for instance, the progressively adopted NIDCAP, Newborn Individualized Developmental Care and Assessment Program [1]).

In order to improve the quality in this aspect of healthcare, some attempts to automatize the detection of neonate's cry have been published. Accurately characterizing the cry in real time could be used in both automatic pain assessment [2] and NIDCAP procedures. In fact, if some neonate in a large NICUs is crying, it could be useful to trigger alarms that request the attention of the nurses.

Regarding methods and techniques to analyze baby's cries, the literature deals with ―neat environment tests‖: only cry sounds are analyzed and, to the sake of our knowledge, proposals do not consider the background noise. This topic attracts the attention of some researches, merely on measuring typical sounds and noises in NICUs and how they affect the well-being of the neonates. In our work, we took a look at papers to get the brief knowledge of background noise in NICUs environments.

1.1. Background

Noise in Neonatal Intensive Care Units For cry analysis in NICUs, background noise is an important aspect which is taken into account. Background noise can come from several sources, namely equipment or machines in hospital rooms, ventilator systems, sounds generated when interacting with incubators, staff talking, phone ring, alarm noise, etc. There are some standards about noise level, for example the standard of American Academy of Pediatrics. If the noise level inside NICUs exceeds these standards for a long period, it will cause some problems on newborns, it can affect neurodevelopment or other important aspects.

In [3] authors describe these environments in terms of background noise, in a recent contribution. Measures were conducted in both an old and a new hospital. Their sound environment was surveyed for 24-hour periods in Melbourne and compared to Australian recommendation, which states maximum and minimum sound levels. For instance, the maximum sound level should be less than 65 dB and no more than 6 minutes in an hour. They also consider sound peaks (defined as jumps of more than 12 decibels). The granularity for noise measuring is 5 seconds, for which averages of decibels are computed. The results show that in general, that recommendation is not achieved in a half of observation periods and the results are not different from the old building to the new one. Moreover, in [4] authors assess background noise according to American Academy of Pediatrics, which recommends that sound levels should not exceed the maximum acceptable level of 45 dB. Authors concluded that the sound environment in the NICUs is louder than most home or office environments and contains disturbing noises of short duration and at irregular intervals. Elevated levels of speech are needed to overcome the noisy environment in the NICU, thereby increasing the negative impacts on staff, newborns, and their families. High noise levels are associated with an increased rate of errors and accidents, leading to decreased performance among staff. The aim of interventions included in this review is to reduce sound levels to 45 dB or less. This can be achieved by lowering the sound levels in an entire unit, treating the infant in a section of a NICU (i.e. in a ―private‖ room), or in incubators in which the sound levels are controlled, or reducing the sound levels that reaches the individual infant by using earmuffs or earplugs.

Finally, in [5] authors describe background noise both quantitatively (measuring sound) and qualitatively (by means of interviews). They compare data collected during day and night periods and conclude that there is no statistically significant difference.

1.2. Contribution and Plan of this Paper

In this paper we analyze the robustness of a cry detection method against real-life sounds that occur in a Neonatal Intensive Care Unit. Then, we implement a method using deep learning, described in Section 2, that is an upgrade of our previous research in the same topic. In Section 3, we test this implementation using audio samples from a cry database, mixed with real audio samples of NICU's background noises then compare to result of old method. Finally, Section 4 concludes de paper.

II. A CRY DETECTION METHOD

In this section the method implemented for cry detection is described. The goal of the method is to detect cry sounds in the waves obtained in the real neonatal intensive care unit (NICU). For the sake of simplicity, we have implemented a software that analyses the recorded waves. However, in a real deployment of the system, it would be able to analyze the sound over real-time acquired audio.

2.1. Key concept

Cry analysis methods make use of several concepts or techniques that play a key role in the process. Sampling is the first step in analysis of audio from real environments. Sounds to be analyzed are in the form of samples of b bit resolution (usually, b=16 for generic audio and b=8 for voice-targeted applications). Samples are taken at a specific sampling rate (being 44.100 Hz a typical value for generic audio and 8.000 Hz the value for voice-targeted applications). Hence, sampling consists of the reduction of a continuous-time signal to a discrete-time signal. Most audio analysis applications rely on frequency estimation. In this step, a window is applied to select a certain interval of data to analyze. Normally, a cry duration has the minimum length of 200 ms, so that the window size normally is 50 ms. After determining the window size, a set of data is collected consecutively from the sampling data set which is obtained from the sampling step. Then, a time to frequency transformation technique, such as Fast Fourier Transform, is applied. Besides sampling and frequency estimation, the following concepts play a key role in the reviewed cry analysis techniques [6, 7, 8]:

- **Fundamental frequency.** Is the most significant frequency contribution of the analyzed audio sample. In terms of frequency analysis of periodic waves, it is the lowest frequency in the sum.

- **Short time energy (STE).** It is the average value of the samples, considering its absolute value, for a generally short number of samples. This granularity is related to the precision of the implementation.

- **Melodic shape.** It is the result of the observation of successive values of fundamental frequencies. Hence, the raising and falling of the cry sound can be characterized by analyzing the features of this melodic shape.

2.2. Description of the Method

The method works with a WAVE audio file. We assume that it has been obtained using a high sensitivity microphone placed next to the incubator. The audio file is recorded at a sampling rate of r samples per second, b=16 bit. The file is divided into a succession of N windows $\{w_1, w_2, \ldots, w_N\}$ of length S, being the latter a parameter of the system. Thus, wi is a succession $\{s^i_1, s^i_2, ..., s^i_S\}$ of samples.

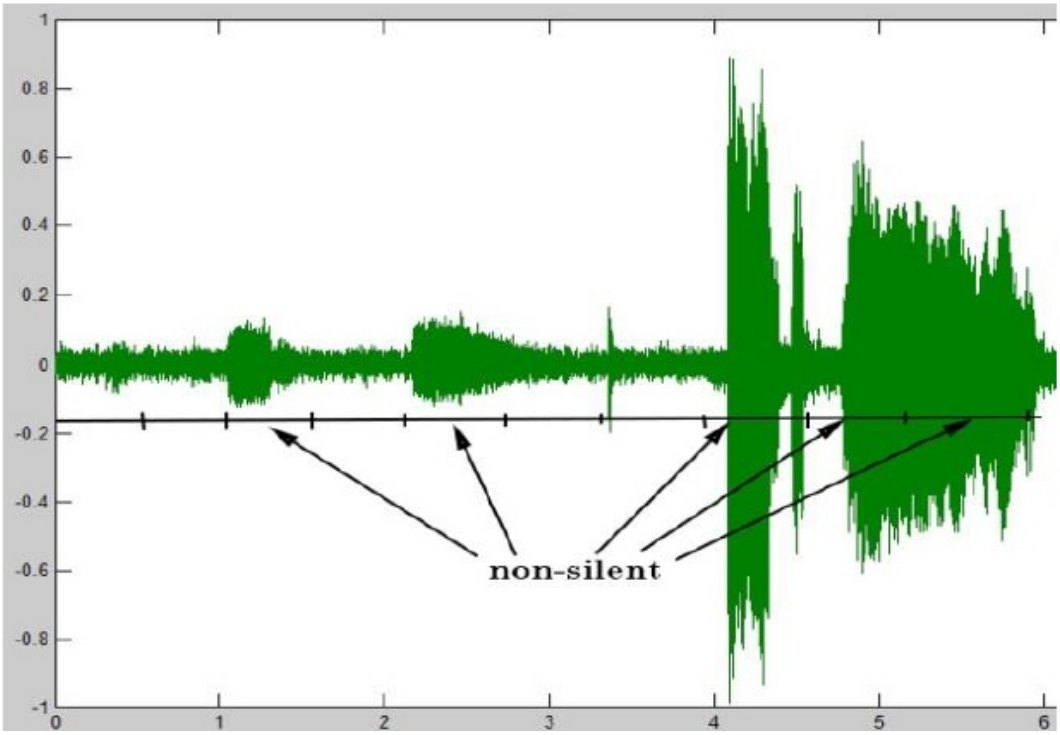

Figure 1: Filter non-silent by sound energy

STE formula:

$$STE(wi) = \frac{1}{S}\sum_{j=1}^{S}(sj)^2$$

The first step consists of detecting a succession of non-silent windows. Note that several successions might be found in a file, but each succession will be analyzed individually. In order to classify a wi into silent or non-silent, the STE is utilized. Then, if STE (w_i)>T , i.e. a specific threshold, wi is classified as non-silent, otherwise it is considered a silent window and therefore is discarder for further analysis.

The problem in the first step is related to detecting as non-silent window sound samples that belong to a near source of background noise. For instance, if a breathing machine is working next to the incubator, the microphone will record this noise but with a high STE. In order to avoid this problem and, assuming that cry frequencies are between 150 Hz and 900 Hz ([6]), we might proceed with a preprocessing. Preprocessing consists of eliminating from wi all the frequencies that according to [6] do not belong to cry. Naturally, higher frequencies pass the filtering and, as a result, this sound could be confused with cries. To that end, a second step analysis, that considers the entire succession of non-silent windows, is mandatory.

In the second step we analyze the entire succession of non-silent windows. This succession's length is L, and is variable in length. The goal of the second step is to compare the wave of the non-silent windows succession with the waves in a so-called Cry Dictionary. The Cry Dictionary contains the wave features of several newborn cries, each with different durations, and in terms of fundamental frequencies.

Hence, in this second step, the fundamental frequencies of each window are obtained. As a result, a succession F of L fundamental frequencies $\{f_1, f_2, \ldots, f_L\}$ is obtained. In this step, we apply a filter algorithm to eliminate the fundamental frequency less than 150 Hz. Because the main purpose of our

method is detecting cry unit in background noise environment, we only care about the fundamental frequency related to cry fundamental frequency. The fundamental frequency of background noise after filtering step can have values in the range of cry fundamental frequency, but it never has the shape of changing in frequency like cry. Finally, the Artificial Intelligent (AI) tool based on deep learning is applied to classify the window is whether cry unit or not. The algorithm is described in Figure 2:

In this method, the input is Audio file (WAV format) recorded by the microphone in real NICU. After processing in our method, the output are: cry units, background windows, silent windows. More specific at the classification step, to build up the AI tool based on deep learning, we use the cry dictionary standard as the training data set from The Baby Chillanto Data Base. This is a property of the Instituto Nacional de Astrofisica Optica y Electronica – CONACYT [9], Mexico and has been used in the literature to assess proposals on cry detection and characterization. Then, to training the Neural Network, the back propagation algorithm is applied.

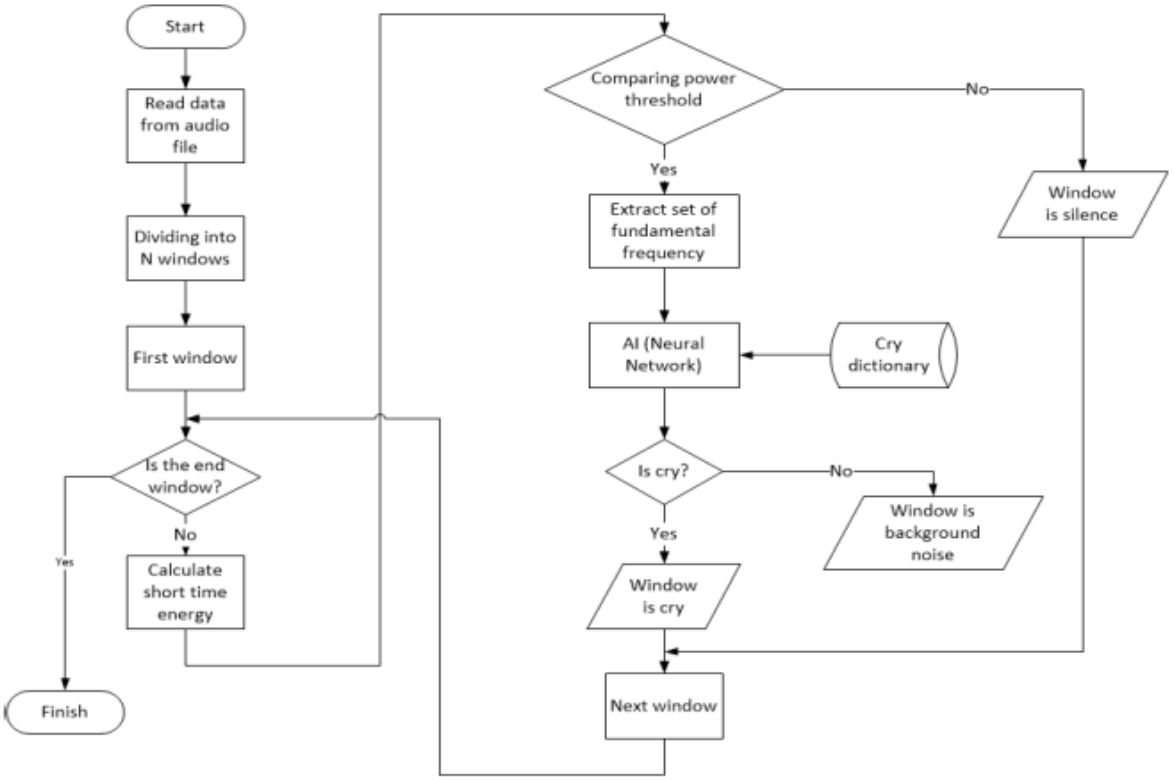

Figure 2: Cry detection methodology using deep learning

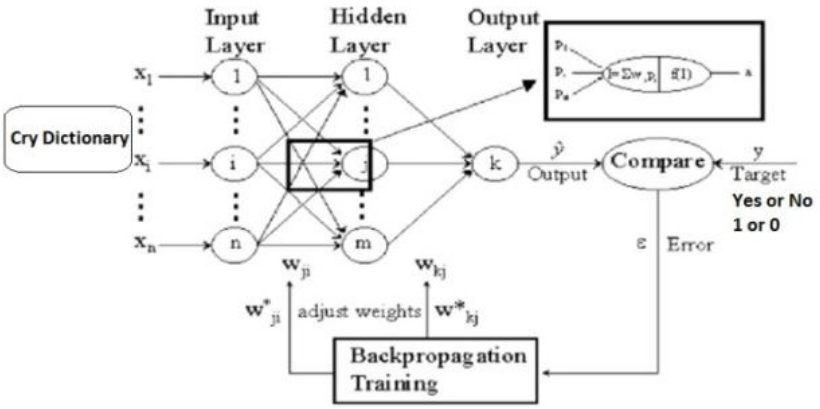

Figure 3: Backpropagation algorithm

III. EXPERIMENTAL RESULTS

The aim of experimental results is to assess if the cry detection algorithm implemented detects sounds not related to cry (e.g. machinery, conversations…) as false cries. Hence we have tested our implementation with neonatal cries in the scenario of a real NICU. 3.1. Sound Samples for Testing Sound samples used for testing have been generated using separate samples for background noise and newborn cries. On the one hand, it is not straightforward to obtain a representative sample of newborn cries. We have selected four samples from The Baby Chillanto database, namely ―Normal_Cry_1‖, ―Normal_Cry_2‖, ―Pain_Cry‖ and ―New_Cry‖. The three first samples have been used to build the Cry Dictionary.

Background noises have been recorded in a real NICU scenario: the neonatal unit in Hospital Universitari Joan XXIII. Samples, with a duration of 10 seconds each, were recorded during November 2016 using a high-sensitivity cardioid condenser microphone and an audio interface attached to a Mac Book Pro. Samples have been recorded by Audacity software. We have selected the following background noise samples:

- "Plain NICU noise‖, background noise that includes humming of the machinery in the unit.
- "Alarm NICU noise‖, background noise that includes an alarm sound.
- "Conversation NICU noise‖, background noise that includes a conversation between adults.
- "Children NICU noise‖, background noise that includes some little girl speaking.
- "Telephone NICU noise‖, background noise that includes a telephone ringing sound and the voice of a nurse attending the call.

In order to generate the final samples that are used in the tests in this work, we have mixed cry sounds with the background noise at different proportions. Specifically, 80% cry plus 20% background and 50% cry plus 50% background. As a result, we test our algorithm with 5 x 3 x 2 = 30 samples with a duration of 10 seconds. For each sample, we know the exact time in which cry starts and, hence, a false positive (i.e. false cry) will consist of detecting a cry outside the boundaries of the parts of the sample where we know the real cry is.

3. 2 Robustness against NICU Noise

Tests have been conducted using a laptop equipped with a core i5-5200U processor and 4GB DDR3 RAM. Each sample took around 3-5 seconds to be evaluated. In this result, the accuracy (in time) is calculated by Total time of cry in detection/Total time of cry in one benchmark. Of course, we also consider these cry units are at the correct position. Tables 1, 2 and 3 show some of the results, for the sake of brevity. To assess the accuracy of our method, we use the accuracy formula:

$$P = \frac{N_{rs}}{N_r} \times 100\%$$

Where:

- N_{rs} is number of accurate unit cries detected from our method.
- N_r is number of unit cries based of our observer.

For the "Normal_Cry_1" (Table 1) tests no false positives were found and, thus, our method is shown to be valid since it does not consider noises as cries. For the "Normal_Cry_2" (Table 2) the result of detecting in first situation of mixing with proportion 20 – 80 % is quite good, there is no False positive in this situation. However, for the second case of mixing with proportion of 50 – 50 %, there exists false positive. The minimum distance of frequency when false positive occur is 150 and this value could

contribute to fine tune our detection algorithm using the Cry Dictionary and our current simple detection method. Finally, in the case of "Pain_Cry" (Table 3) the results are optimal since no false positives have been detected.

Sample	AI		Frequency distance	
	Accuracy(%)	False Positive	Accuracy (%)	False Positive
20_80_Alarm_Noise_Normal_Cry_1	98	No	91	No
20_80_Conversation_ Noise_Normal_Cry_1	92	No	82	No
50_50_Alarm_Noise_Normal_Cry_1	88	No	73	No
50_50_ Telephone _ Noise_Normal _Cry_1	80	No	54	No

Table 1.Some representative results in the case of "Normal_Cry_1".

Sample	AI		Frequency distance	
	Accuracy (%)	False Positive	Accuracy(%)	False Positive
20_80_Alarm_Noise_Normal_Cry_2	82	No	62	No
20_80_Conversation_Noise_Normal_Cry_2	80	No	54	No
50_50_Alarm_Noise_Normal_Cry_2	60	No	25	No
50_50_Telephone_Normal _Cry_2	70	No	35	Yes

Table 2.Some representative results in the case of "Normal_Cry_2".

Sample	AI		Frequency distance	
	Accuracy (%)	False Positive	Accuracy (%)	False Positive
20_80_Alarm_Noise_Normal_Cry_1	100	No	100	No
20_80_Conversation_Noise_Normal _Cry_1	100	No	100	No
50_50_Alarm_Noise_Normal_Cry_2	96	No	86	No
50_50_Conversation_Noise_Normal _Cry_2	90	No	72	No

Table 3.Some representative results in the case of "Pain_Cry".

3.3.Detection of a Cry not in the Dictionary

Until now, we have described the success of our method in terms of not detecting false positives. In addition, we consider assessing the validity and robustness of our method about detecting new cries that are not in the dictionary. To that end, we have tested our method using the fourth sample from the database, and creating mixes with background noise from the real NICU. Table 4 shows that out method gives does not detect false positives and detects the new cry as well.

Sample	Cry Interval	False Positive
NewCry_Plain _Noise	4.2 - 6.0 6.4 - 7.2	No
NewCry_Telephone_Noise	4.0 - 4.6 4.8 - 5.8 6.2 - 7.2	No

Table 1.Results in the case of "New_Cry".

3.4. Discussion

In most of the cases, our method can correctly detect cry regardless the background noise, even in case of mixing 50 % of noise. Comparing to the previous method of frequency distance, the deep learning method yields better results, from at least 8% to 35%. The deep learning way also avoids false positive which exists in the previous one.

In case of “Normal_Cry_1" and “Pain_Cry”, which we already know are the good cry recording, the quality of the method is correct. It gives very high accuracy in case of 20 – 80 % of mixing noise. In “Normal_Cry_1" case, it always gives the accuracy more than 80 %. In case of “Pain_Cry”, the result is even better, around 100 % of accuracy. In case of “Normal_Cry_2", we knew that this file -i.e. the sample from the cry database , it also contains a noticeable amount of background noise. Thus the detecting result is not good as the others. In situation of 20 – 80 % mixing background noise, it only gives the result with accuracy around 80 %, but in situation of 50 – 50 % mixing background noise, the result is even worse. It is not good enough to become the standard for detecting cry.

The result in the situation of mixing 20 – 80 % mixing background noise is always better than the result in the situation of mixing 50 – 50 %. In case of “Normal_Cry_1" and “Pain_Cry”, situation of 20 – 80 % gives result of over 80 % and nearly 100 % respectively. But the situation of 50 – 50 % is only gives result of average 60 % and 80 % respectively. In case of “New Cry”, our method gives a good result of detecting cry. There is no false positive in this case even the amplitude of noise is quite high. It can detect the most important cry signals correctly.

IV. CONCLUSION AND FUTURE WORK

In this paper we have addresses the robustness of cry detection techniques against real-life neonatal intensive care units. Our method has correctly detected cry regardless background noise. In our work, we determined that fundamental frequency is the most important feature of newborn infant cry. Thus, we focused on characterizing the feature of the changing and the shape in fundamental frequency. Comparing to the other method, and our previous method, it could reduce the computational cost but still gives us the good result.

Although we get good result in detecting cry unit in most of the case, but some situations can be improved. The reason is insufficient quality of Cry Dictionary. The cry sample with the name “Normal Cry 2" containing noise inside, when creating standard cry unit from it, it reduces the quality of the Cry Dictionary. In future, we will investigate more about building the good and standard Cry Dictionary for better training and make it to be a good benchmark for other researches.

In our method, the value of some importance parameters which are power threshold is still not fixed. Because we do not have the standard scenario for recording cry, the cry samples are mixed by other audio software. In near future, we will design a standard scenario, the device for recording cry of the newborn infant will be put near the incubator to warranty that the background should have the lower energy than the cry. In this work, we just implemented the basic method to classifying cry unit based on deep learning and Neural Network. It can be still improved because fundamental frequency is not the unique characteristic of cry unit. In the future, we will implement other artificial intelligent method like Supported Vector Machine, etc to classify cry unit based on the set of input attributes including fundamental frequency, some resonance frequencies and average power frequency ratio. The new method will take into account all the features of cry signal, thus, the quality of cry detection should be improved.

ACKNOWLEDGMENTS

This paper was completed by financial supporting from IOIT project (Institute of Information Technology) of Vietnam Academy of Science and Technology (VAST): ―Researching the cry detection method in real neonatal intensive care units.‖ which project's code is: CST20.01.

REFERENCE

[1] O. J. Bedrij, ―Carry-select adder,‖ IRE Trans. Electron. Comput, pp. 340–344, 1962.

[2] B. Ramkumar, H.M. Kittur, and P. M. Kannan, ―ASIC implementation of modified faster carry save adder,‖ Eur. J. Sci. Res., vol. 42, no. 1, pp.53–58, 2010.

[3] T. Y. Ceiang and M. J. Hsiao, ―Carry-select adder using single ripple carry adder,‖ Electron. Lett., vol. 34, no. 22, pp. 2101–2103, Oct. 1998.

[4] J. M. Rabaey, Digtal Integrated Circuits— A Design Perspective Upper Saddle River, NJ: Prentice-Hall, 2001

[5] J. M. Rabaey, Digtal Integrated Circuits— A Design Perspective Upper Saddle River, NJ: Prentice-Hall, 2001.

[6] Y. He, C. H. Chang, and J. Gu, ―An area efficient 64-bit square root carry-select adder for lowpower applications,‖ in Proc. IEEE Int. Symp. Circuits Syst., 2005, vol. 4, pp. 4082–4085.

[7] Cadence, ―Encounter user guide,‖ Version 6.2.4, March 2008

(ISSN NO. (Print) : 2347-6982, (Online): 2349-204X)

Electricity Demand Forecast Error Mitigation in A Fast Charging Station

[1] Nikhil Singhal, [2] Hasan Ashraf, [3] Richa Yadav, [4] Mohd Waqas
[1]4th Year Mechanical Engineering Student, GGSIPU, Delhi, India
[2]4th Year Mechanical Engineering student at GGSIPU, Delhi India
[3]4th year Electrical and Electronics Engineering Student, GGSIPU, Delhi, India
[4]4th Year Mechanical Engineering Student, GGSIPU, Delhi, India
E-mail: Hasanashraf141414@gmail.com

ABSTRACT

The highlighted global energy crisis and environmental degradation have significantly boosted the development of electric vehicles(EVs), Compared to gasoline-powered vehicles, EVs can dramatically reduce the greenhouse gas emission, energy cost for drivers, and dependencies on imported petroleum. As the trend for electric vehicles is increasing day by day the load on power stations are also increasing. Due to this high-level uncertainty in EV it may bring about deleterious impacts to the electric grid. Therefore, an advanced system is needed to overcome this problem. Therefore, in this paper we proposed an advanced demand forecast method which can calculate the expected EV charging load in FCSs. If we are able to predict the approaching vehicles, we can ensure the energy needed for the same. Firstly, the wavelet transform (WT) method and long short-term memory (LSTM) neural network are combined to predict the non-stationary traffic flow (TF). Then, a queuing theory-based model is developed to convert the predicted TF to the expected EV charging demand in FCS by considering charging service limitations and driver behaviors.

Keywords - Electric Vehicle, Fast Charging Station, Energy Storage System

I. INTRODUCTION

The highlighted global energy crisis and environmental degradation have significantly boosted the development of electric Vehicles (EVs). Compared to gasoline-powered vehicles, EV scan dramatically reduce the green house gas emission, energy cost for drivers, and dependencies on imported petroleum [1,2]. Generally, EVs can be charged either in a normal charging mode at their destination, e.g., home and workplace, or in a fast charging mode at fast charging stations (FCSs) [3, 4]. Due to the short charging time, fast charging technology has recently attracted a lot of attention and FCSs are expected top lay an important role in the widespread use of EVs in the near future[5]. Because an FCS is usually connected to a distribution network, it shares power capacity with other loads, and the EV charging demand forecast error due to a high level of uncertainty in EV loads may bring about deleterious impacts to the electric grid. Application of forecast in FCSs can provide an effective measure to address this issue. Therefore, it becomes increasingly important to develop an advanced system for above problem.

This paper is devoted to mitigating EV charging demand forecast error impacts. The main technical contributions are summarized as follows: (1) a novel TF forecast model is proposed by combining the Wavelet Transform (WT) method and Long Short-Term Memory (LSTM) neural network to effectively extract nonlinear features of TF data and thereby obtain a superior prediction performance. (2) An improved queuing model is constructed by considering service limitations of FCSs and the inherent to chasticity of driver behaviors to derive the EV charging demand in FCSs.

II. FAST CHARGING STATION DEMAND MODELING

A.LSTM Neural Network

Recurrent neural networks (RNNs) introduce the concept of timing to the traditional neural network structure to make it adaptiveto time horizon dependencies. However, due to the vanishing and exploding gradient problems, traditional RNNs arenotoriously difficult to train properly. To alleviate such training-related complications, Hochreiter et al. [9] proposed an LSTMneural network that can learn long-term dependent information in sequences. An LSTM neural network consists of a series ofLSTM cells and the time series data samples are simultaneously fed into different LSTM cells as inputs. Fig. 2 illustrates theinternal structure of an LSTM cell.

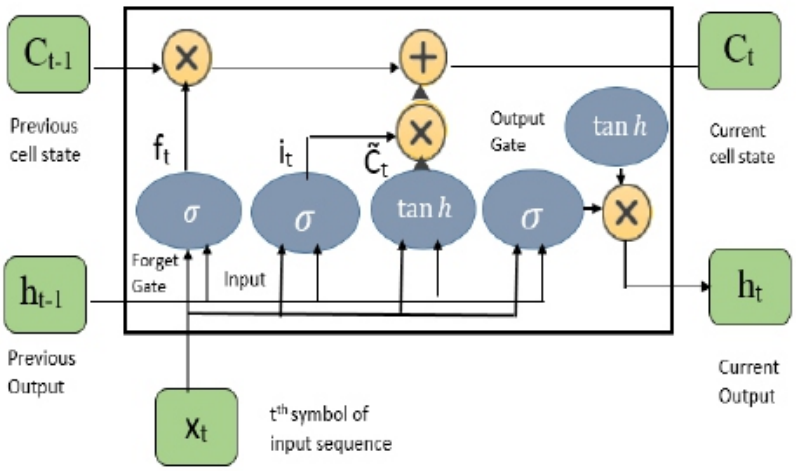

Fig. Internal System of an LSTM cell

The forward propagation process of LSTM neural network training can be described as follows. The LSTM cell state is denoted by Ct. LSTM uses forget, input and output gates to control the addition and removal of the cell state information. Each gate is a neural network layer with a sigmoid activation function whose output value is between 0 and 1, dictating how much of each component should be let through for pointwise multiplication with the cell state. The calculation processes of forget, input and output gates can be expressed as follows.

$$f_t=\sigma(W_f[h_{t-1},x_t]+b_f)$$
$$i_t=\sigma(W_i[h_{t-1},x_t]+b_i)$$
$$o_t=\sigma(W_O[h_{t-1},x_t]+b_O)$$

Where σ is the sigmoid activation function; ht-1 is the hidden layer output; x_t is the input sequence vector at time t; W_f, W_i, and W_o are the weight matrices for forget, input and output gates respectively; b_f, b_i, and b_o are the biases of different gates. Then, a current candidate cell state is calculated by using the tanh activation function and shown as (4), where W_C and b_C are the weight and bias of tanh layer of the input gate respectively.

$$C_t = \tanh(W_C[h_{t-1},x_t]+b_C)$$

The proportions of information occupied by the C_{t-1} and C_t in the current cell state C_t are determined by the forget gate and Input gate, respectively. The state C_t is updated as:

$$C_t = f_t \cdot C_t\text{-}1 + i_t \cdot C_t$$

Finally, the current output of the hidden layer is obtained as:

$$h_t=o_t \cdot \tanh(C_t)$$

B. LSTM Neural Network-Based Traffic Flow Prediction

Considering the influence of the chaotic nature of TF data on prediction accuracy, a novel TF prediction model is developed based on the WT method and LSTM neural network. Its implementation flowchart is presented in Fig. 3.

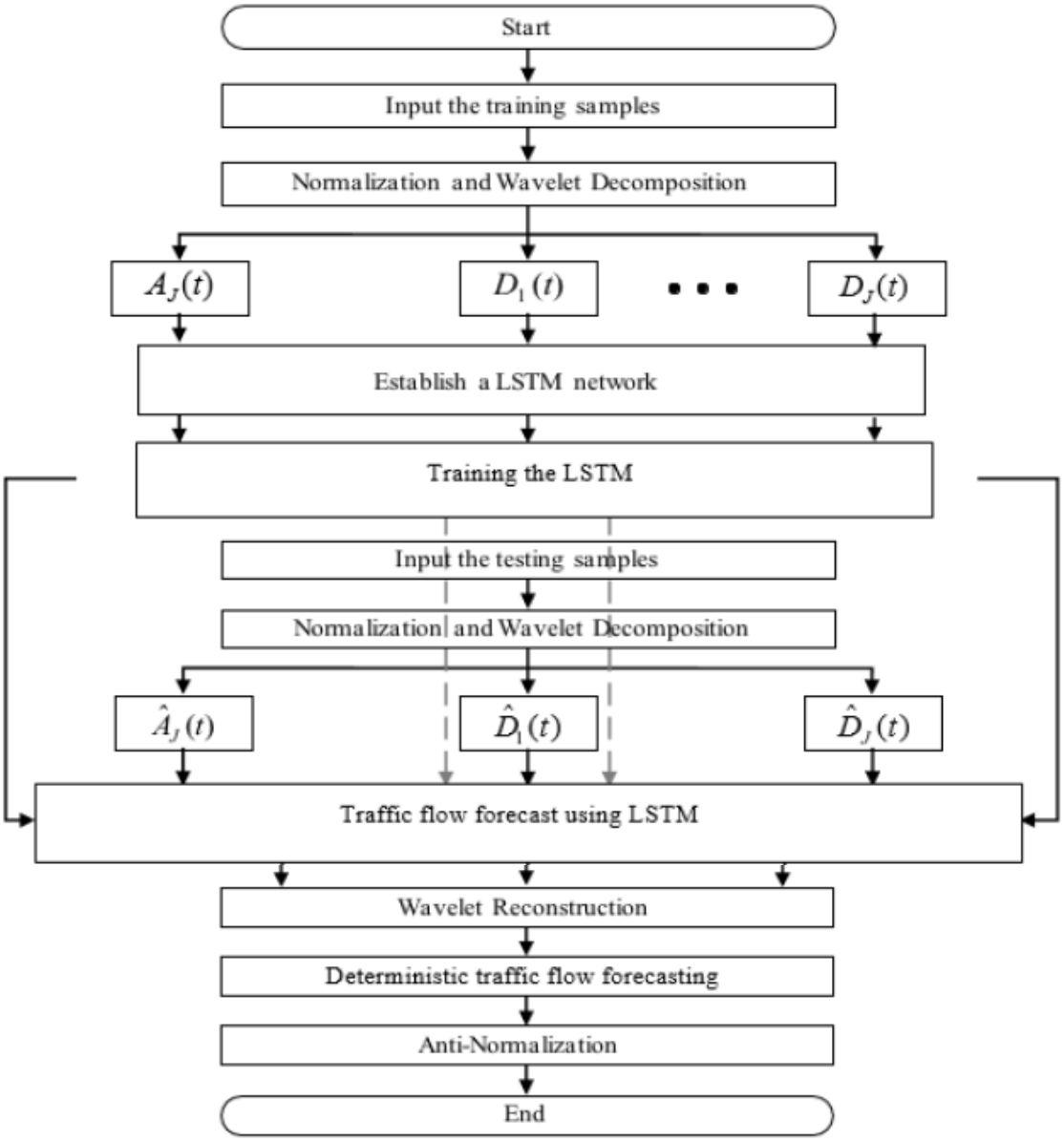

Fig. Flowchart of WT-LSTM neural network-based traffic flow prediction

If the original TF data are directly used as the inputs of the LSTM neural network, their non-linear and non-stationary characteristics will inevitably deteriorate TF forecasting accuracy. To address this issue, the original TF data is normalized to the passenger car unit (pcu) and then decomposed by using a fast discrete WT algorithm that can simultaneously provide the time and frequency information of the TF data series. The discrete-time WT of a given signal g(t) can be defined as [10]:

$$W(m,n)=2^{-0.5m}\sum_{t=0}^{T-1} g(t)\,\psi(2^{-m}t-n)$$

where ψ(·) is the mother wavelet; t is the discrete-time index; T is the length of the signal g(t); m and n represent two integer variables that determine the parameters of scaling and translation of the mother wavelet respectively. Through the multi-scaledecomposition, the original TF sequence is decomposed into an approximate signal, AJ(t), and multiple detail signals, {D1(t),…,DJ(t)}.

Thereafter, the normalized and wavelet decomposed training instances are fed into multiples LSTM neural networks to extract the essence characteristics of TF data. The disparity between the predicted component obtained from LSTM neural network, ˆt y ,and the observed one, yt, is represented by the following loss function at the end of each forward propagation.

$$L = \frac{1}{T}\sum_{t=0}^{T-1}(y_t - \hat{y}_t)^2$$

Then, the time-back propagation algorithm [10] is used to update the network weights and biases based on the gradient of the loss function until the convergence criteria are met. During testing, a forward propagation is solely required to generate the estimated components of TF data at each time step and no backward propagation is needed since the network parameters have been already learned during training. Although the forward propagation is comprised of a series of matrix multiplications, the training process is typically conducted offline. Thus, LSTM neural network is less computationally intensive than other algorithms.

Finally, the predicted components are integrated through the wavelet reconstruction and then denormalized to obtain the forecasting result of TF.

C. EV Charging Demand Prediction with Queueing Theory

To determine the charging demand at an FCS, the EV arrival rate is an important parameter and should be properly estimated. Generally, the EV arrival rate at FCS changes with the traffic flow data. For the sake of simplicity, in this paper, it is assumed that an average of φ EVs per 100 vehicles will enter the FCS for charging service, then the arrival rate of λ of EVs can be calculated as follows, where y denotes the number of vehicles driving on the road per unit time.

$$\lambda = y \times \left(\frac{\varphi}{100}\right) \times 100\%$$

In practice, the parameter φ can be determined based on the dynamic travel behaviours and state of charge (SOC) conditions. Next, the EV charging demand at an FCS is estimated with the EV arrival rate and an improved M/M/s/K queueing theory. As shown in Fig. 4(a), EV owners may require waiting at an FCS to recharge their EV batteries.

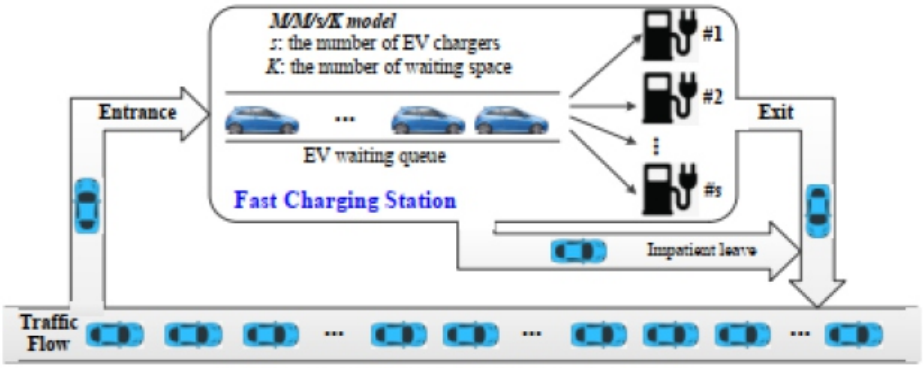

(a) The workflow of fast charging station

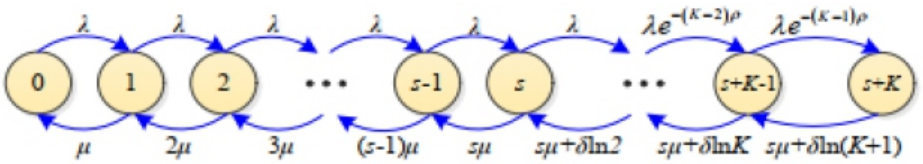

(b) State transition diagram of Markov chain

Fig. M/M/s/K queueing model of fast charging station

The adopted M/M/s/K queue is a multi-server queue with s identical EV chargers and a maximum queueing length of K. In the FCS, all EV chargers work independently and the EVs are served based on a first-come-first-serve rule. If all the waiting spaces are occupied, the charging request from EVs is rejected. In such M/M/s/K model, EV arrivals follow a Poisson process with an EV arrival rate λ, and EV charging duration obeys an exponential distribution with an average charging duration 1/μ, where μ is the average EV leave rate for each time interval.

Based on the above rules, the probability that an EV chooses to join the queue can be expressed as:

$$\alpha_k = \begin{cases} 1 & k < s \\ e^{-(k-s)p} & s \le k < s+k \\ 0 & k = s+K \end{cases}$$

Where k is the number of EVs in FCS, and $\rho > 0$ is a parameter that defines the probability decrease rate. Besides, some impatient EV owners in the queue may choose to leave the FCS and find nearby FCSs to charge their vehicles, and their number during each time interval can be assumed as:

$$\beta_k = \begin{cases} 0 & k < s \\ \delta \ln(k-s+1) & s \le k < s+K \end{cases}$$

Where the logarithm function, $\ln(\cdot)$, suggests the β grows with the increase of k, and δ is a sensitive parameter that defines the intensity of leaving. In practice, the parameters, i.e., ρ and δ, can be obtained according to the analysis of historical queueing data or some specific experiments. According to (10) and (11), the average arrival rate, λ_k, and average leaving rate, μ_k, of EVs in FCS can be calculated as follows:

$$\lambda_k = \lambda\alpha_k = \begin{cases} \lambda & k < s \\ \lambda e^{-(k-s)p} & s \le k < s+k \\ 0 & k = s+K \end{cases}$$

$$\mu_k = \begin{cases} k\mu & k, s \\ C\mu + \beta_k & s \le k < s+k \end{cases}$$

Based on the Markov chain of the M/M/s/K model in Fig. 4(b), the FCS balance equation is expressed as:

$(\lambda_k + \mu_k)P_k = \lambda_{k-1} P_{k-1} + \mu_{k-1} P_{k+1}$

Where P_k *denotes* the probability that there are k EVs in the FCS, and $\sum_{k=0}^{s+K} P_k = 1$

By solving (14),

probability P_k is derived as:

$$P_k = \begin{cases} \left(\frac{\varsigma^k}{k!}\right) P^0, & 0 \le k \le s \\ \frac{\varsigma^k e^{-0.5\rho(k-s)(k-s-1)}}{s!\prod_{i=1}^{k-s}[s+\eta \ln(i+1)]} P_0 & s < k \le s+K \end{cases}$$

Where $\varsigma = \lambda/\mu$, $\eta = \delta/\mu$, and P_0 is:

$$P_0 = \left[\sum_{k=0}^{s}\left(\frac{\varsigma^k}{k!}\right) + \sum_{k=s+1}^{s+K} \frac{\varsigma^k e^{-0.5\rho(k-s)(k-s-1)}}{s!\prod_{i=1}^{k-s}[s+\eta \ln(i+1)]}\right]^{-1}$$

Finally, the EV charging demand at the FCS, PFCS, can be determined as (17) with the charging EV number, $N_{EV,}$ and the charging power of the chargers, P_{EV}.

$$P_{FCS} = N_{EV} P_{EV} = \left(\sum_{k=0}^{s} kP_k + s\sum_{k=s+1}^{s+K} P_k\right) P_{EV}$$

V. CONCLUSION

In this paper, we have tried to solve the overloading on power grids due to high use of electric vehicles. This problem is solved by predicting the number of vehicles coming on electric stations. At first, a prediction model considering service restrictions in FCS and driver behaviour was established to determine the expected charging demand of EVs at the station. In this model, the WT method and LSTM neural network were combined to improve the TF prediction accuracy. We then used a novel queuing model to simulate the charging behaviours and obtain the predicted demand in FCS. This method will not only help in predicting the vehicles approaching but in future it can also help in making sure that we have enough power on stations to meet the people needs.

REFERENCE

[1] T. Wu, Q. Yang, Z. Bao, and W. Yan, "Coordinated energy dispatching in microgrid with wind power generation and plug-in electric vehicles,"IEEE Trans. Smart Grid, vol. 4, no. 3, pp. 1453-1463, Sep. 2013.

[2] H. Zhang, S. J. Moura, Z. Hu, W. Qi, and Y. Song, "A second-order cone programming model for planning PEV fast-charging stations,"IEEE Trans. Power Syst., vol. 33, no. 3, pp. 2763-2777, May 2018.

[3] X. Gan, H. Zhang, G. Hang, Z. Qin, and H. Jin, "Fast-charging station deployment considering elastic demand,"IEEE Trans. Transport. Electrific., vol. 6, no. 1, pp. 158-169, Mar. 2020.

[4] H. Zhang, S. J. Moura, Z. Hu, and Y. Song, "PEV fast-charging station siting and sizing on coupled transportation and power networks,"IEEE Trans. Smart Grid, vol. 9, no. 4, pp. 2595-2605, Jul. 2018.

[5] S. Negarestani, M. Fotuhi-Firuzabad, M. Rastegar, and A. Rajabi-Ghahnavieh, "Optimal sizing of storage system in a fast charging station for plug-in hybrid electric vehicles,"IEEE Trans. Transport. Electrific., vol. 2, no. 4, pp. 443-453, Dec. 2016.

[6] N. Korolko, Z. Sahinoglu, and D. Nikovski, "Modeling and forecasting self-similar power load due to EV fast chargers,"IEEE Trans. Smart Grid, vol. 7, no. 3, pp. 1620-1629, May 2016.

[7] Z. Duan, B. Gutierrez, and L. Wang, "Forecasting plug-in electric vehicle sales and the diurnal recharging load curve,"IEEE Trans. Smart Grid, vol. 5, no. 1, pp. 527-535, Jan. 2014.

[8] Y. Li, S. Li, and B. Hannaford, "A model-based recurrent neural network with randomness for efficient control with applications,"IEEE Trans. Ind. Inf., vol. 15, no. 4, pp. 2054-2063, Apr. 2019.

[9] S. Hochreiter, and J. Schmidhuber, "Long short-term memory,"Neural Comput., vol. 9, no. 8, pp. 1735-1780, Nov. 1997.

[10] C. Lin, W. Gao, and M. Guo, "Discrete wavelet transform-based triggering method for single-phase earth fault in power distribution systems,"IEEE Trans. Power Del., vol. 34, no. 5, pp. 2058-2068, Oct. 2019.

[11] Y. Zhou, B. W. Ling, X. Mo, Y. Guo, and Z. Tian, "Empirical mode decomposition-based hierarchical multiresolution analysis for suppressing noise,"IEEE Trans. Instrum. Meas., vol. 69, no. 4, pp. 1833-1845, Apr. 2020.

[12] Martinez-Mares, and C. R. Fuerte-Esquivel, "A robust optimization approach for the interdependency analysis of integrated energy systems considering wind power uncertainty,"IEEE Trans. Power Syst., vol. 28, no. 4, pp. 3964-3976, Nov. 2013.

(ISSN NO. (Print) : 2347-6982, (Online): 2349-204X)

Hydrophobicity Class of Porcelain Insulators Base on Information Image Feature Extraction Via Image Processing

[1] Poohthip Sonkaeo, [2] Chanchai Techawatcharapaikul

[1,2]Electrical Engineering Department, King Mongkut's University of Technology, Thonburi, Bangkok, Thailand

E-mail: [1]poohthip.mcguyrever@mail.kmutt.ac.th, [2]chanchai.tec@kmutt.ac.th

ABSTRACT

Nowadays, quality assurance of polymeric outdoor insulators service life is necessary to be checked regularly for use, the hydrophobicity is usually a laborious parameter to determine in this field. Regarding this purpose, image processing by classification by followed the standard IEC TS 62073-2016 [1]from photography on wet areas around insulator surfaces has been the main technique. This paper is the study and construction of a test kit about the effect of hydrophobic levels of insulators. There is testing with the 52-1 porcelain insulator with RTV coating. Here we show that the result of the level of hydrophobic with levels from HC1 – HC7. Moreover, the image processing applications enable to quantify and relate these properties in a mathematical function were found, that could be used in the field by the electrical companies because no human errors are detected and can add conditions to improve algorithm.

Keywords - Classification, Image Processing, Hydrophobicity Class, Insulator

I. INTRODUCTION

From the presence of technology into a role today. Further research needs to be developed to achieve more effective results. The major problem of human experiment work is the error from human eye measurement. The traditional HC examination methods have some defects that require the expertise of the experimenters and enough trial time. Therefore, measurement methods are proposed by using image processing principles to extract various features [2 - 10] instead of human measurements that may cause deviations from the test such as Fractal dimension, Circular factor, Goniometric measurement using Hough transformation, Scaled entropy and Histogram analysis, Surface energy and Online hydrophobicity measurement methodology. However, only 1-2 parameters are used. These methods do not have a comprehensive overview. In addition, research is often focused on improving methods. But the research has not been created as a tool for verifying the actual test results.

For image processing technology [11] it has been suggested for the detection of HC. There are 3 processes which are the image pre-treatment, The image segmentation and classification. In research [12] Adaptive filtering is used to adjust the gradation was applied to the treatment of images of water spray on the insulator surface and the k-nearest neighbor method was used for classification of HC. Next, the research [13] will use Wavelet transform and the hydrophobic images are segmented according to the Threshold. The resistance model was created to analyze the quality of the contamination on the insulator surface and with a combination of test methods classification a variety of steps to distinguish factors from the properties of separation with various techniques. The research [14] is used to extract the properties of the workpiece and statistically including Cosine transformation, Wavelet transformation, Radon transformation, Contour transformation, Gray-scale co-occurrence matrices and Stepwise regression. Classification will be verified by these methods.

Later in the research that [15] after the image processing of insulators. All 7 geometric parameters are separated to better adjust the settings according to the properties related to HC. The model of insulators will increase efficiency reliable to create a Neural network.

The HC classification method from research [16] consists of Template matching, Structure pattern recognition, Fuzzy pattern recognition and Neural networks, and other methods. Template matching method is used with patterned objects to compare with objects. In order to be analyzed with the standard format, which formats have a closer match level. To classify the objects. Structure pattern recognition is a method for finding patterns that are continuously is a simple format arranged to create a Tree shape pattern. This method can prevent interference from various defects, most of which are used in text analysis and image analysis.

II. DETAILS EXPERIMENTAL

2.1. Related Works

The hydrophobic level of insulators applied and developed by designing and installing a test kit. Next, test each experiment, analyze the data and conclusions. Which the image processing algorithm used to analyze the test results. The details of the process used for testing is by the Contact Angle measurement is given in Table 1.

Name	Spray Method
Colour Transformation	•
Edge Detection	•
Noise Reduction	•
Morphological Operation	•
Curve Fitting	•
Component Labelling	•
Classification	•

Table1: The experimental process table.

2.2. Equipment

In the design and installation of the test kit. Space is calculated with 50 × 100 × 90 cm in size so that the experiment kit can support different types of insulators as follows: Class 52-X, 53-X, 54-X, and 57-X. Automatic sliding rail sets for precise control of testing distances and lighting for optimal lighting orientation.

2.3. Spray Methods

This method is spray water to look like mist must be at about 25 cm, with a deviation of no more than ± 10 cm at an angle to the horizontal plane. The duration of spraying must spray for 20 s to 30 s, with the volume of water sprayed about 10 ml to 30 ml and the result must be collected within 10 s after the spray is finished as shown in Fig.1.

Fig. 1. Test kit of Spray Method.

III. EXPERIMENTAL DESIGN

When performing the experiments [9] from the set of experiments that have been created, the results are as follow steps: First, we reconstruct the binary standard template images of 7 HC by divide each standard image from [1] into 9 sub-images for multi resolution images (Original size, Vertical divide, Horizontal divide, and Square divide) which combination of Noise Reduction Process as shown in Fig. 2.

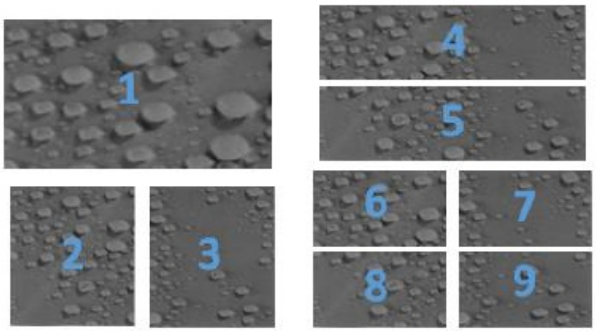

Fig. 2. Divide 9 multi resolution templates (Original size, Vertical divide, Horizontal divide and Square divide)

Next, we construct the initial binary test image by capture the water droplets image on the surface of the insulator which the same standard size specified. After that we use the denoise processing which combine of Morphologically technique and Average Filter as show in Fig. 3

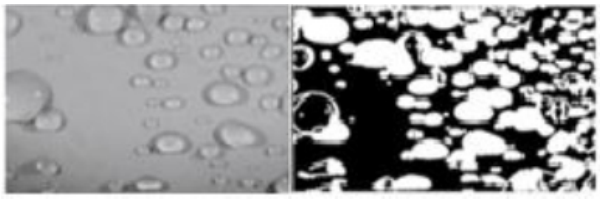

3A) Original test image 3 B) Initial Binary test image

Fig. 3. The initial binary test image

Then, we only focus the main useful information via large among of pixel in each component by use Component Labelling process, the sequence of adjacent pixel groups in both of the binary standard template images of 7 HCin step 1 and the initial binary test image in step 2. Then use the sum of each pixel to calculate the average. To make a comparison between each pixel sum with the average. If the pixel sum is less than the average, it will be an error and will be cut off, but if the pixel results are greater than or equal to the average, data will be kept. "The Finally Binary test image" as show in Fig. 4

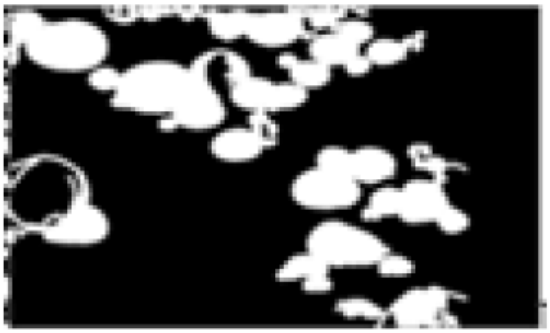

Fig. 4. The finally binary test image

The information for HC Classification is the relative between the "density value" (% ratio of all value pixels and all pixel in image) and "Wet Surface MAX", the maximum quantitative pixel form the quantitative data component in image. After that we construct the model of each HC by the singular value decomposition method (SVD) to get smaller sub-matrix data, where the values of ΣU are made as a master axis variable and ΣV are made as prime axis variables. Then create the ellipse equation to plot the data set in each class. The figure 5 show the relative of "density value" and "Wet Surface MAX" from the binary standard template images of HC as shown in Fig. 5.

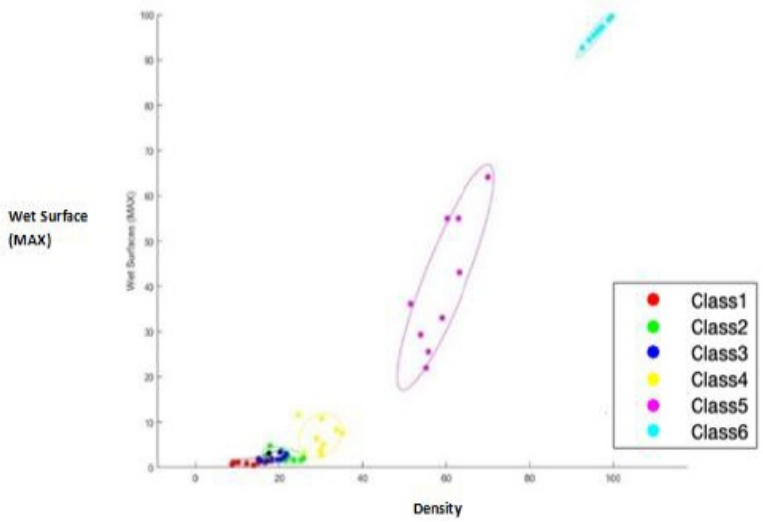

Fig. 5.The final step for find the classification to test the image.

Finally, After plot the classification graph to find the distance between two points, from the center of the ellipse of each class, to the test object (picture from the test insulator) using the Mahalanobis Distance equation and find the smallest distance. For predicting the effect of water droplet image on insulator surface. Which, if the distance of any class is the smallest. Show that the picture of water droplets on the insulator surface is in that class and store the information.

IV. RESULTS

The hydrophobic test of porcelain suspension insulators 52 - 1 by water spray method. Which takes 20 s to spray the water, the volume of the spray is 30 ml, the test area is approximately 50 square cm. The distance from the surface of the insulator to the plane from the distance of 20, 25 and 30 cm, respectively, can be summarized as follows:

Porcelain insulator suspension 52-1, coated with RTV, evaluated Hydrophobicity Classification at HC 2, which, when considered from a perpendicular perspective. Found that the appearance of droplets all over the surface is a water droplet quite round on the surface. And in the spray testing at various distances as specified by the standard. Made known that it does not affect classification.

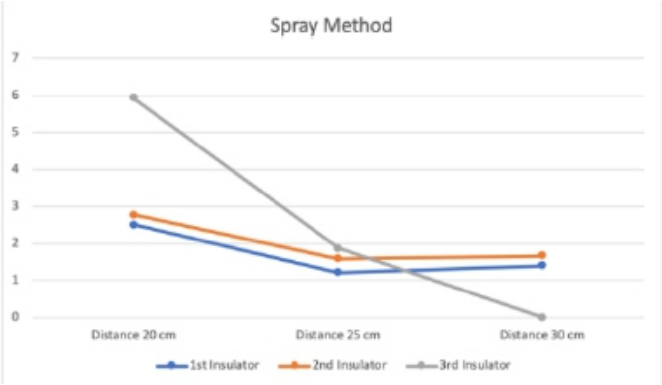

Fig. 9. Graph showing the result of the Contact Angle Method

When comparing the test results, it was found that insulators with RTV coating can evaluate Hydrophobicity Classification. Which has a hydrophobic level from the visual observation and the use of image processing to help classify Classification. Which has a hydrophobic level of 6 Class. It can be concluded that Insulators with RTV coating have a harder wetting surface than HC with a higher-class number than HC 2 and have a wetting surface more easily than HC with a class number lower than HC 2. Therefore, water droplets can adhere on the floor. Good skin texture. In accordance with the standards [1].

V. DISCUSSION AND CONCLUSION

This research is a part of project is based on the experiment of the hydrophobic. of insulators. Type of porcelain insulator hanging 52 - 1 with 3 RTV coating. The test method will be in accordance with the requirements of the IEC TS 62073 - 2016 by testing method for measuring the image feature extraction of water droplets on the insulator surface From the test results, it is found that the equipment is usable in hydrophobic testing. and can be concluded that:

Method for measuring the Spray Method. Insulators coated with RTV have a dense wet area and the density of the wettest area is close to the HC 2. So, it can be estimated at the HC 2 level. which shows the level of at high hydrophobicity, the surface of the insulator is therefore hydrophobic. So, it can be estimated at the HC 2 level. which shows the level of at high hydrophobicity, the surface of the insulator is therefore hydrophobic.

From the experiment, the RTV coating on the insulator surface. As a result, in insulators having the level of hydrophobic (High hydrophobicity) that drops of water will adhere to the surface of the insulator or the surface of the insulator is difficult to get wet, which causes the skin flashover is caused by insulators

in wet or humid skin conditions and contaminated with water to become a conductor on the surface of the insulator.

rom the experiment, the RTV coating on the insulator surface. As a result, in insulators having the level of hydrophobic (High hydrophobicity) that drops of water will adhere to the surface of the insulator or the surface of the insulator is difficult to get wet, which causes the skin flashover is caused by insulators in wet or humid skin conditions and contaminated with water to become a conductor on the surface of the insulator.

ACKNOWLEDGMENT

This work was supported, in part, by advice, collecting data and helping for set an experiment. The authors also would like to thank Mr. BoonnuaPungsiri, Mr. RamesSronwiset and Mr. Siratan Khinawong from the Thailand University of King Mongkut's University of Technology Thonburi.

REFERENCE

[1] International Electrotechnical Commission. IEC62072 Guidance on the measurement of wettability of insulator surfaces. Geneva; 2016.

[2] Swedish Transmission Research Institute – STRI. Guide 92/1 Hydrophobicity Classification Guide; 1992.

[3] Hartings R. Hydrophobicity of composite insulators: measurement and influence on flashover performance. In: Proceedings of the Stockholm Power Tech: International Symposium on Electric Power Engineering. New York, USA: Royal Institute of Technology; 1995

[4] Gubanski S and Hartings R. Swedish research on the application of composite insulators in outdoor insulation. Electrical Insulation Magazine. 1995Gubanski S and Hartings R. Swedish research on the application of composite insulators in outdoor insulation. Electrical Insulation Magazine. 1995

[5] Tokoro T, Nagao M and Kosaki M. Image analyses of hydrophobicity of silicon rubber insulator. In: Annual Report Conference on Electrical Insulation and Dielectric Phenomena. Texas, USA:Institute of Electrical and Electronics Engineers; 1992

[6] Altafim RAC, Santana AM, Murakami CR, Basso HC, Chierice GO and Neto SC. Hydrophobicity of polyurethane resins. In: Proceedings of the International Conference on Solid Dielectric. Toulouse, France: Institute of Electrical and Electronics Engineers; 2004.

[7] Zhao L, Li C, Xiong J, Zhang S, Yao J and Chen X. Online hydrophobicity measurement for silicone rubber insulators on transmission lines. IEEE Transactions on Power Delivery. 2009

[8] Li Z, Liang X, Zhou Y, Tang J, Cui J and Liu Y. Influence of temperature on the hydrophobicity of silicone rubber surfaces. In: Proceedings of the Annual Report Conference on Electrical Insulation and Dielectric Phenomena. Colombia: Institute of Electrical and Electronics Engineers; 2004

[9] Yang, L.; Bi, J.K.; Hao, Y.P.; Nian, L.P.; Zhou, Z.J.; Li, L.C.; Liao, Y.F.; Zhang, F.Z. A recognition method of the hydrophobicity class of composite insulators based on features optimization and experimental verification. Energies 2018

[10] Yang, L.; Bi, J.K.; Hao, Y.P.; Nian, L.P.; Zhou, Z.J.; Li, L.C.; Liao, Y.F.; Zhang, F.Z. A recognition method of the hydrophobicity class of composite insulators based on features optimization and experimental verification. Energies 2018

[11] Breg, M.; Thottappillil, R.; Scuka, V. Hydrophobicity estimation of HV polymeric insulating materials development of a digital image processing method. IEEE Trans. Dielectr. Electr. Instrul. 2001

[12] Peng, K.; Wang, Q.; Wang, X. Spray image analysis-based measurement of hydrophobic of insulator surface. Insul. Mater. 2005

[13] Zhang, Z.Y.; Yan, K.; Wang, F.C.; Yang, S.J.; Li, N.C. Insulator hydrophobic identification method based on image feature extraction and BP neural network. High Volt. Eng. 2014

[14] Jarrar, I.; Assaleh, K.; El-Hag, A.H. Using a pattern recognition-based technique to assess the hydrophobicity class of silicone rubber materials. IEEE Trans. Dielectr. Electr. Insul. 2014

[15] Yang, L.; Bi, J.K.; Hao, Y.P.; Nian, L.P.; Zhou, Z.J.; Li, L.C.; Liao, Y.F.; Zhang, F.Z. A recognition method of the hydrophobicity class of composite insulators based on features optimization and experimental verification. Energies 2018

[16] Yin, Q.G.; Yang, Z.K.; Tan, Z. Pattern Recognition and Neural Networks; Machinery Industry Press: Beijing, China, 2003

(ISSN NO. (Print) : 2347-6982, (Online): 2349-204X)

Implementation of Weather Sensor Interfaced System Basedon Field Programmable Gate Array (FPGA)

[1] Poe Zar Chi Aung, [2] Tin Thetnwe, [3]Myint Myint Than
[1,2,3]Department of Electronic Engineering Yangon Technological University, Yangon
E-mail: ecdepartment.ytu@gmail.com

ABSTRACT

This paper presents the hardware design and implementation of weathers on Field Programmable Gate Array (FPGA). The sensor is useful for sensing weather that can measure multiple parameters and especially developed for mobile applications and wearables where size and low power consumption. The system offers the extremely fast response time and also supports performance requirements for developing applications such as high accuracy over a wide temperature range. The design based on Serial Peripheral Interface (SPI) for serial communication. SPI is the most commonly used serial protocol for low/medium bandwidth data transfer and supports full duplex mode. This configuration has been described using VHDL (VHSIC Hardware Description Language).FPGA NEXYS 4 DDR from Digilent has been used for the hardware implementation and has been simulated by Xilinx Vivado Software tools. The system can be used in weather station to measure temperature, pressure and humidity.

Keywords - SPI, FPGA, Sensor, VHDL description language, Vivado

I. INTRODUCTION

BME280 sensor is an environmental sensor which can sense temperature, barometric pressure, and humidity. It is reliable for weather sensing that measures humidity with ±3%, barometric pressure with ±1hPa, and temperature with ±1 degree Celsius. The sensor has been used with SPI communication with FPGA. FPGA is an integrated circuit silicon chip that can be configured by the user to emulate any digital circuit as long as there are enough resources [5]. It can be seen as an array of Configurable Logic Blocks (CLB) connected through programmable interconnects and also can be reprogrammed to desired application or functionality requirements after manufacturing [1]. Serial Peripheral Interface (SPI) is a short distance serial communication protocol which enables synchronous transmission of data in full duplex mode. SPI is 4-wire synchronous serial data protocol and the advantage of SPI is used for connecting low speed external devices using four wires. It was leaded as a serial communication interface between a microcontroller and its peripherals. It is suitable interface for embedded systems and now can also be used directly to configure FPGA from SPI sensor [3]. In this system, the FPGA is the master device and the SPI sensor acts as the slave device. The system has been designed using VHDL description and tested using Xilinx Vivado Software. The finite state machine (FSM) is used to perform a predetermined sequence for the system [4]. II. BACKGROUND In this study, it is described some background information to design and verification of serial data from sensor in VHDL.

A. SPI Protocol

SPI is a single-master protocol. This implies that that one central device or process, a master, controls and initiates all the communications with one or more other devices or processes, known as slaves. The protocol uses at least four signal lines: a clock signal (SCLK), a data line from slave to master (MISO), a data line from master to slave (MOSI) and a chip select signal (CS) for each slave in the system. When

the master wishes to send data/ request information from a slave, it selects the slave by pulling down the matching CS-line. Data is read through the MISO line and sent through the MOSI line[2]. The data from Master device is transmitted to slave device by MOSI and received by MISO as shown in Figure.1.

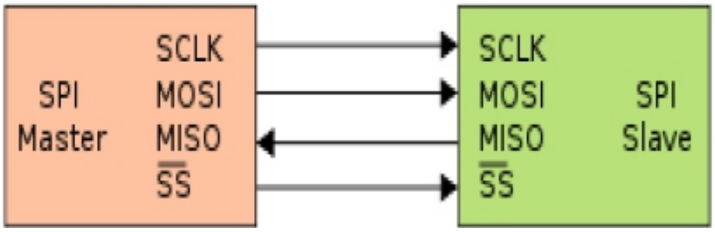

Figure 1. Block Diagram of SPI

There are four mode of SPI interface as shown in Table.1.

Mode	CPOL	CPHA
0	0	0
1	0	1
2	1	0
3	1	1

B. BME280 Sensor

It has 6 pinouts for SPI:

1. Vin - Power pin
2. GND – Common ground for power logic
3. SCLK – SPI clock pin
4. MOSI – Serial data out pin that send from BME280 to FPGA
5. MISO – Serial data in pin that send from FPGA to BME280
6. CS – Chip Select pin, drop it low to start an SPI transaction

Figure 2. BME280 Sensor

C. Nexys4 DDR FPGA Board

Field-Programmable Gate Arrays (FPGAs) are the low cost, power and performance. The structure of the FPGA produces to implement any sequential and combinational circuits, which can reprogram separately at different frequencies than the microcontroller. It can be reconfigured into a master controller, a soft processor and a simple logic function. The FPGA is used CAD tools or Hardware

Description Languages (HDL) such as VHDL and Verilog HDL to program. FPGAs can accomplish the calculation of numerous types of algorithms in terms of speed and power consumption in comparison to microcontrollers of sensor nodes[3].

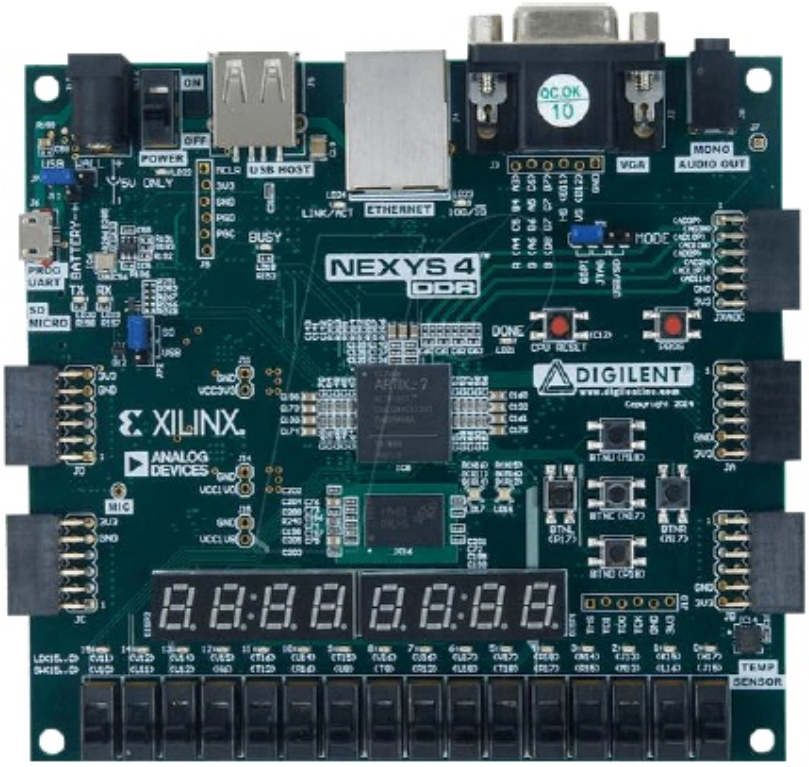

Figure 3. Nexys4DDR FPGA Board

The Digilent Nexys4 DDR board is based on Artix-7 FPGA and is compatible with Xilinx‟s high-performance Vivado Design Suit. Therefore, designs can be implemented at low cost. The Nexys4 DDR board includes 7-segment LED displays that can perform the digit values by arranging one of 128 patterns and an LED is embedded in each segment [6]. The 7-segment LED displays are used in this system to show the hexadecimal values.

III. METHODOLOGY

The block diagram for implementation of BME280 sensor using SPI interface is shown in figure 4.

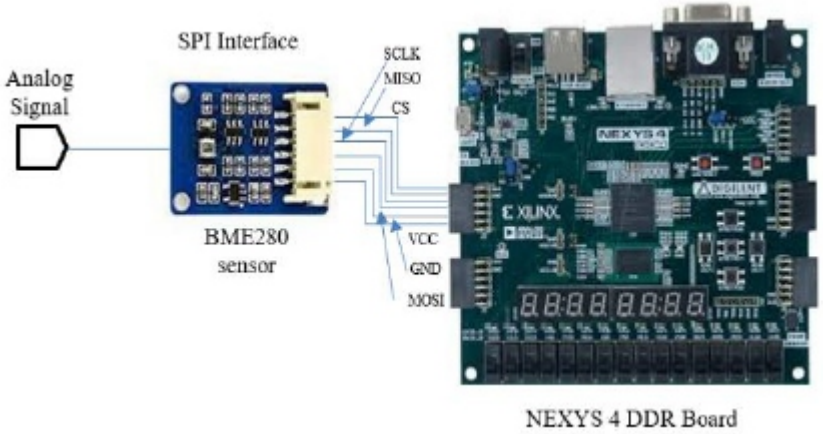

Figure 4. System diagram of the system

The system consists of the interface between FPGA and BME280 sensor. The FPGA, the master unit, sends SCLK clock, the required register address via MOSI output and CS chip select output to the sensor. Then the sensor unit, the slave, produces the raw ADC serial sensor values to FPGA via MISO pin. The overall system is coded by VHDL description. The destination register is controlled by FSM (Finite State Machine). The following Figure 5 shows how to read raw ADC sensors values and it is the top FSM design. The following figure shows the SPI communication with the sensor.

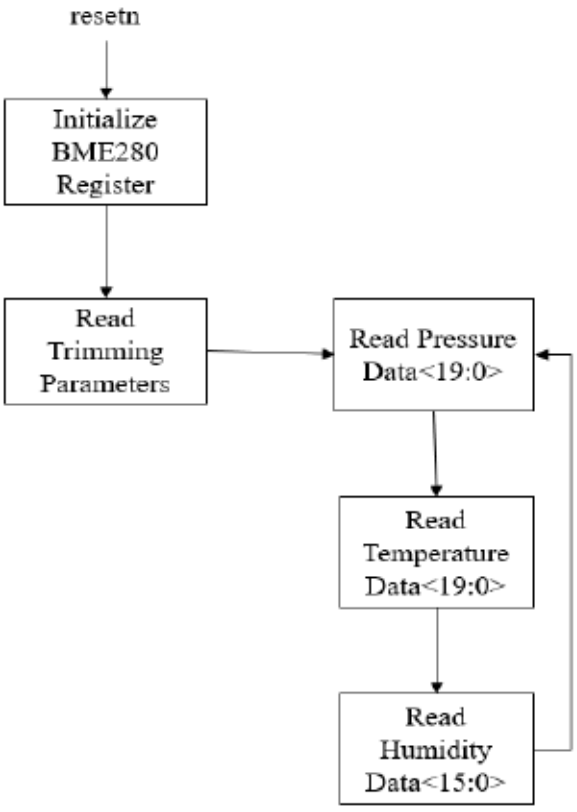

Figure 5. SPI FSM Design

Figure 6. shows the simulation results for the FSM state of SPI protocol in VHDL. At the Idle state, CS is logic „0" and count is set to „0". At the control write 1 state, CS is „0" and count is added by one and the necessary command register address values are shifted out via MOSI pin to the sensor module. When CS is „1", it has reached at the Stop 1 state. At the control write state, CS is „0" again and count is added by one and also the other necessary command values are shifted out via MOSI pin to send the temperature register address. At the data read state, the 20-bits of temperature values from sensor is shifted out via MISO pin. At the calculate state, the actual temperature values are calculated using a set of calibration parameters with 20-bits of binary values. When CS is „1", it is gone to stop3 state. When load is off, the system is returned to Idle state.

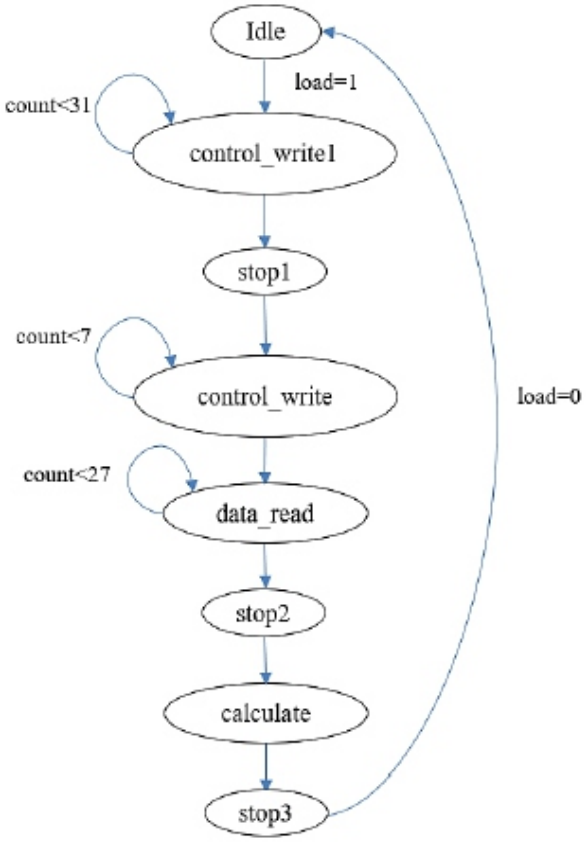

Figure 6. FSM for the system

Figure 7. shows which takes a register address as a parameter and reads a byte from that register. It begins to drive the chip select line low. Once this is done, a byte is sent to theBME280 specifying the register address and making sure bit 7 is high. For a write operation, bit 7 should be low as shown in Figure 8. When the register address is sent, it is depending on data read or write.Data is sent out the MISO pin, the register is automatically incremented.[5]

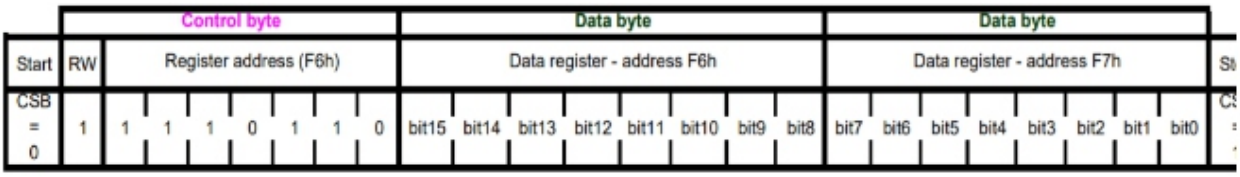

Figure 7. SPI multiple bytes read

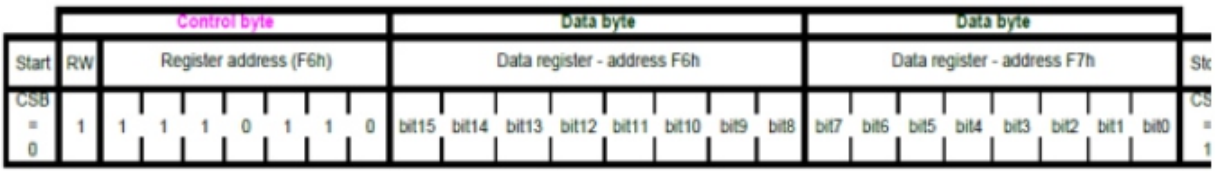

Figure 8. SPI multiple bytes write

IV. TEST AND RESULTS

In this section, we are going to showthis simulation result of SPI sensor implementation in FSM states is shown in following Figures.The system of SPI interface is compatible with SPI mode „11“ (CPOL =CPHA= „1“) and mode „00“ (CPOL= CPHA = „0“). Therefore, this system is used mode „00“. The input frequency of FPGA board is 100 MHz.Therefore, the SCLK input frequency is 200 Hz that is divided by clk_divider in VHDL design.

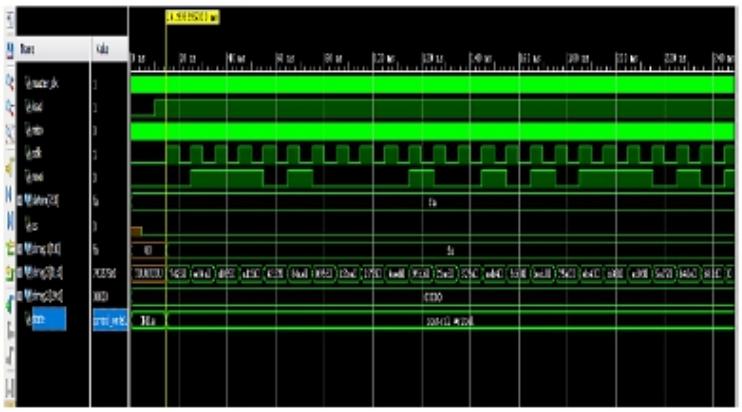

Figure 9. Simulation result of Idle and control_write1 state

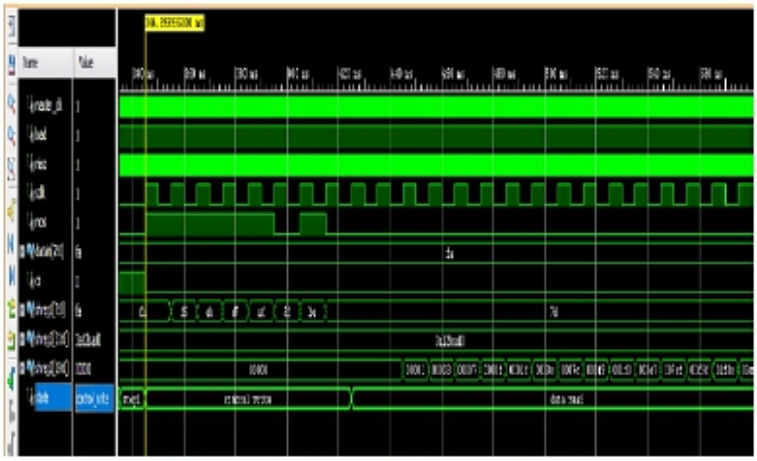

Figure 10. Simulation result of control_write state

Figure 11. Simulation result of data_read state

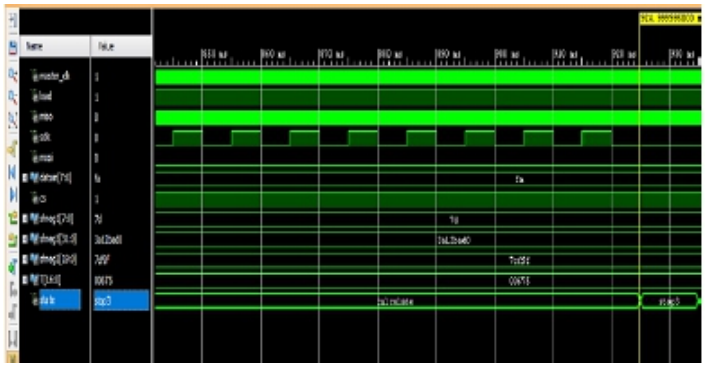

Figure 12. Simulation result of calculate state

When CS is „0" in Idle state, CS is „0" and count is initially zero in. At the control write1 state, 32_bits of control data register are shifted via MOSI pin as shown in figure 9. At control write state, the 8_bits of register address from FPGA switches are sent to sensor in figure 10. In the same sequence, the digital output data are shifted from MISO pin at the data read state as shown in figure 11. Then, figure 12 shows that the 20_bits output data values are calculated using calibration data from sensor. When load goes low, it is returned to Idle state.

Register Address (LSB/MSB)	Name	Value	Type
0x88 / 0x89	dig_T1	28760	U16
0x8A / 0x8B	dig_T2	26792	S16
0x8C / 0x8D	dig_T3	50	S16
0x8E / 0x8F	dig_P1	37630	U16
0x90 / 0x91	dig_P2	-10555	S16
0x92 / 0x93	dig_P3	3024	S16
0x94 / 0x95	dig_P4	7964	S16
0x96 / 0x97	dig_P5	-105	S16
0x98 / 0x99	dig_P6	-7	S16
0x9A / 0x9B	dig_P7	9900	S16
0x9C / 0x9D	dig_P8	-10230	S16
0x9E / 0x9F	dig_P9	4285	S16

Table 2. Calibration data of BME280 sensor

Table 2 shows the calibration data of BME280 sensor that are programmed into the sensor device by the factory and the user cannot change this value. The corresponding compensation data are named dig_T for temperature and dig_P for pressure. Each 8-bits registers are stored at memory addresses 0x88 to 0x9F.The actual temperature and pressure values are calculated using a set of calibration parameters. The BME280 has three different measurement modes; normal, forced and sleep mode. Forced mode was chosen, as it tells the sensor to only registers new values when command so by the FPGA, thereby minimizing energy costs. When delivered from the factory, the sensor is by default set to sleep mode, not making any measurements. To start measuring, the pressure and temperature oversampling rate of the given measurement type needs to be set to at least x1 and the measurement mode has to be changed.This was however not described in the documentation, and had to be found out by testing different values and settings. All settings of the sensor are changed by writing to different register.

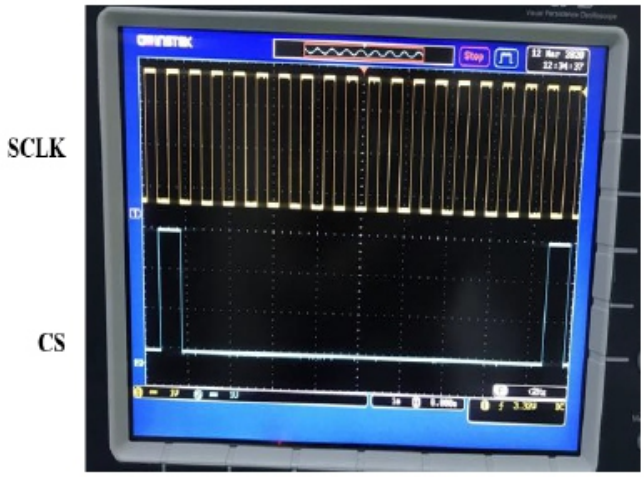

Figure 13. Result of sensor data from oscilloscope

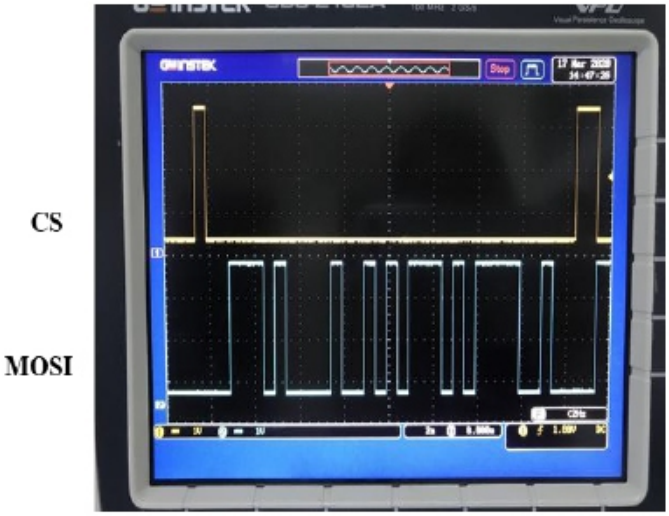

Figure 14. Result of sensor data from oscilloscope

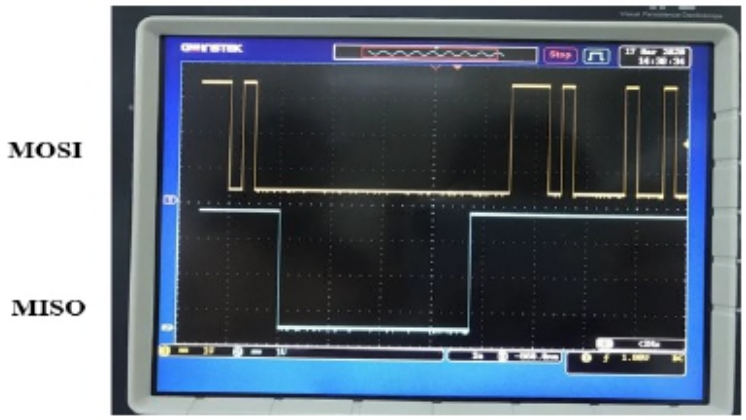

Figure 15. Result of sensor data from oscilloscope

Figure 13 show the sensor data of serial clock and chip select. The transaction starts the CS falling state. Figure 14 shows that control data transmitted from the master is sent to the MOSI pin of the SPI bus at the data transfer state. Figure 15. shows the data from slave sensor is sent to the MISO pin of the SPI bus at the data transfer state 2.

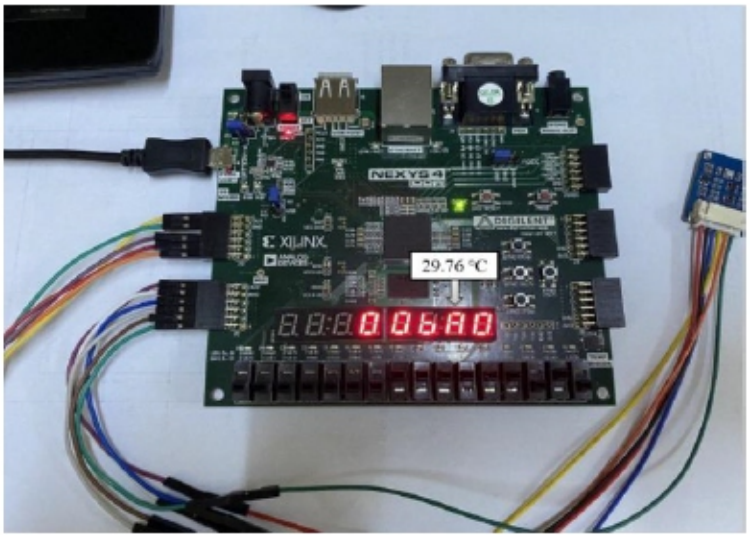

Figure 16. Result of actual temperature value in 7-segment

Figure 16 shows the hexadecimal value at room temperature. The hexadecimal value, BA0H is converted to decimal value, 2976D that is multiply with 0.01℃ resolution to get the actual temperature value. Hence, the result is 29.76℃. When the sensor is heated with fire, the result of temperature value is increased as shown in figure 17. The hexadecimal value, DA5H is converted to decimal value, 3493D and the result is 34.93℃.

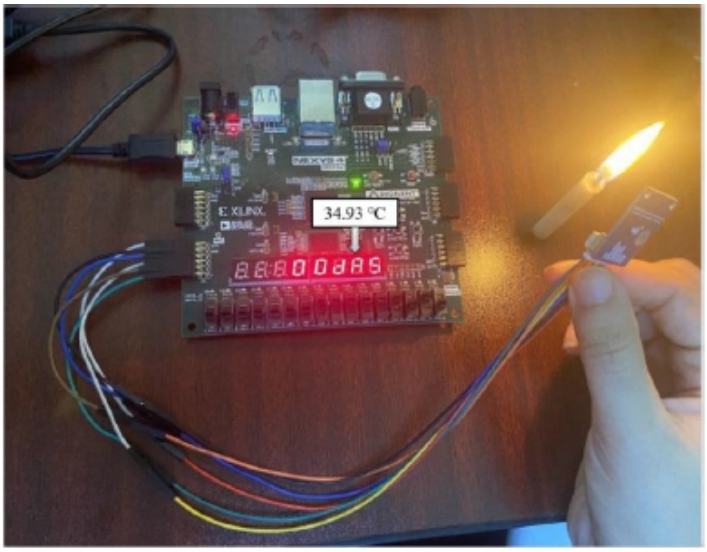

Figure 17. Result of actual temperature value in 7-segment

V. CONCLUSION

This study presents the implementation of BME280 sensor interfaced system based on FPGA, which is reconfigurable, desires less power consumption and has more efficiency.Serial Peripheral Interface (SPI) is implemented for real time communication in this research. The advantages of BME280 sensor can sense three values of sensing data, temperature, pressure and humidity. The FPGA-based platform is a low-cost early validation platform. As a future work, the pressure and humidity data are sampled and measured could be displayed in LCD with FPGA board.

REFERENCE

[1] J. M. Jasso, G. O. Vargas, R. C. Miranda, E. V. Ramos, A. Z. Garrido, G. H. Ruiz, "FPGA based Realtime remote Monitoring system", Journal of Computers and Electronics in Agriculture, V 49, 2005, p 272–285.

[2] TruptiD.Shingare, R.T.Patil."SPI Implementation on FPGA". International Journal of Innovative Technology and Exploring Engineering (IJITEE), Volume-2, Issue-2, January 2013.

[3] Xilinx Inc., 7 Series FPGAs Data Sheet: Overview, DS180 v2.4 Product Specification (2017).

[4] Iuliana CHIUCHISAN, Alin Dan POTORAC, Adrian GRAUR. "Finite State Machine Design and VHDL coding techniques". 10th International Conference on Development and Application Systems, Suceava, Romania, May, 2010.

[5] Bosch Sensortec. BME280 Sensor Datasheet

[6] Digilent, Inc., Nexys4 DDR FPGA Board Reference Manual (2016)

(ISSN NO. (Print) : 2347-6982, (Online): 2349-204X)

Performance of Solar Air Conditioning

Guermit. Tahar
Faculty of Applied Sciences, Department of Mechanics, University Kasdi Merbah of Ouargla (Algeria) E-mail: Tguermit56@gmail.com

A B S T R A C T

Pressurized mechanical cooling technologies are used in our refrigerators and air conditioners. But the energy consumed by this technology is very high and results in high consumption of electrical energy. The absorption machine is the most used. An absorption cooling machine is a machine that requires little maintenance and no consumption of electrical energy, especially when a circulation pump is not used in the system. The use of solar thermal energy to power an air conditioning system. Among these possibilities, the absorption solar air conditioning technique is the most commonly used.

Keywords - Performance, Absorption Refrigeration, Air Conditioning, Solar.

I. INTRODUCTION

The use of solar energy in sunny countries is an effective way to compensate for the lack of energy especially in rural areas where it is sometimes difficult and expensive to supply them with the electricity grid. Also, Algeria is a country in which there is strong solar radiation in several regions. It is important to exploit this natural resource in the field of cold production, especially in the absorption machine for air conditioning because of its simplicity of design and implementation [1]. The interest of solar air conditioning lies in the simultaneity of the demand for cooling and the sunshine. When the heat necessary for the operation of the absorption refrigeration machine is supplied by solar energy, thus lower cost and no pollution, the solar air conditioning system can be an interesting solution. Solar air conditioning refers to all air conditioning techniques using solar energy as a primary energy resource. Use of solar thermal energy to supply an air conditioning system by evaporation or by desiccation (solid or liquid). Among these possibilities, the absorption solar air conditioning technique is the most commonly used ... In solar air conditioning, the binary water-lithium bromide pair (LiBr / H2 O) is often adopted. [2]

II. SOLAR ABSORPTION REFRIGERATION MACHINES

In this system, flat solar collectors are used to vaporize the refrigerant. A solution composed of a pair of refrigerant liquid and absorbent liquid is brought to the boil inside the sludge trap thanks to the thermal input of thermal solar panels. The pressure increases and the refrigerant evaporates as it separates from the absorbent. The refrigerant vapours are directed to the condenser where they release their heat by cooling upon contact with ambient air; the condensates of the refrigerant are relaxed to access the low-pressure area of the installation; the refrigerant in the liquid state is directed into the evaporator where it vaporizes instantly, taking the calories from the room to be cooled. Together, the "refrigerant-poor" absorbent solution is withdrawn from the sludge trap via an expansion valve to supply the absorber. The refrigerant vapours brought into contact with this solution are then absorbed. The refrigerant-absorbent pair thus regenerated is returned to the sludge trap by a pump. The cycle can then start again. [3].

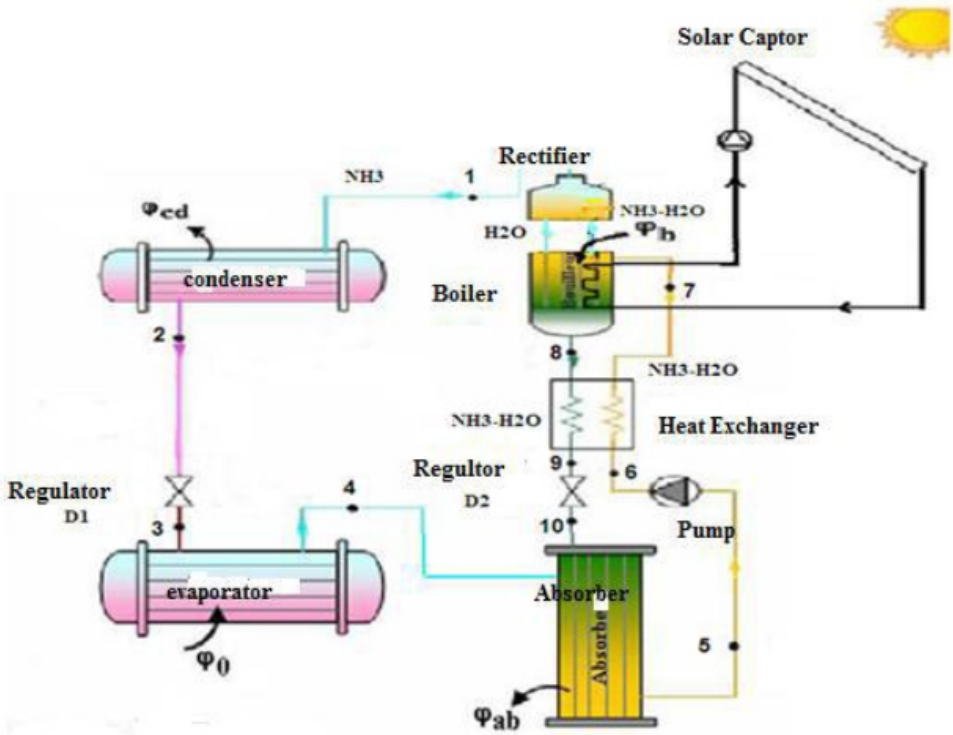

Fig1: solar absorption refrigeration machine

The most common technique is to use solar collectors to provide heat which is directed to an absorption machine. This machine dissociates, by boiling, a solution of water and lithium bromide. After cooling, the recombination of the two components produces cold, by absorption of heat. The cold is then distributed as for conventional air conditioning. [4]. The efficiency of the sensor can be further improved by using a selective surface for the absorber, which makes it possible to obtain a strong absorption of solar radiation and low infrared emission, and insulating glasses also make it possible to reduce thermal losses. the balance in terms of primary energy consumption is favourable to the solar cooling system if at least 51% of the cooling demand can be satisfied by solar energy. To assess the economic viability of the system, energy prices and investment costs should be taken into account.

On the other hand, it could be considered for a building where the cold demand is limited to the summer months thanks to an adequate design (solar protection, valorization of thermal inertia).

III. THERMODYNAMIC ANALYSIS

The performance of an absorption refrigeration machine depends on the chemical and thermodynamic properties of the fluids used. In this section, we present the equations necessary for the calculation of the thermodynamic properties [5][6].:]The refrigerant:Saturation pressure

$$P(T) - 10^3 \times \sum_{i=0}^{6} a_i \times (T - 273.15)^i$$

(III.1)

The enthalpy of the saturated liquid *h*l calculate by

$$h_l(T) = \sum_{i=0}^{6} b_i \times (T - 273.15)^i$$

(III.2)

The enthalpy of saturated vapour *h*v calculates by:

$$h_v(T) = \sum_{i=0}^{6} c_i \times (T - 273.15)^i$$

(III.3)

The solution: The relationship between the saturation pressure the temperature and the concentration of the ammonia-water mixture is given by

$$logP = A - \frac{B}{T} \qquad \text{(III.4)}$$

$$A = 7.44 - 1.767.\ x + 0.9823.\ x^2 + 0.3627.\ x$$
$$B = 2013.8 - 2155.7.\ x + 1540.9.\ x^2 - 194.7.\ x^3$$

$$h(T,X) = 100 \sum_{i=0}^{16} a_i \times \left(\frac{T}{273.15} - 1\right)^{m_i} \times \bar{X}^{n_i} \qquad \text{(III.5)}$$

X is the mole fraction of ammonia in the mixture

Coefficient of performance COP [7]:

Using the previous equations, the coefficient of performance can be expressed as

$$COP = \frac{Q_{evap}}{Q_{gén} + Wp} \qquad \text{(III-6)}$$

Assuming that the work of the pump on the rich solution is negligible compared to the other terms, the coefficient becomes

$$COP = \frac{Q_{evap}}{Q_{gén}} = \frac{mf(h4 - h3)}{mfh1 + mgh8 - mah7}$$

Finally

$$COP = \frac{(h4 - h3)}{(h1 + ((FR - 1)h8) + (FR)h7)} \qquad \text{(III-8)}$$

Remember to check the spelling. If your native language is not English, please get a native English-speaking colleague to proofread your paper.

IV. RESULTS AND DISCUSSION

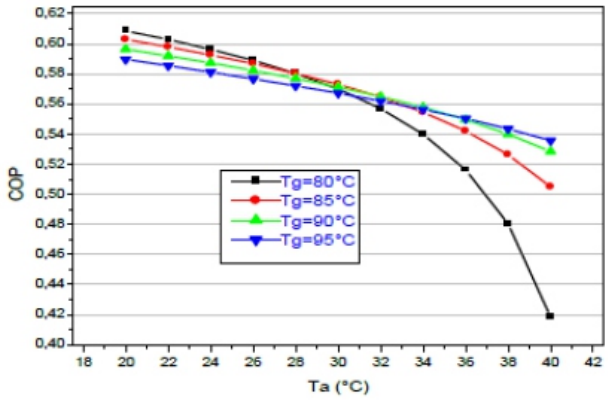

Fig 2: variation of COP as a function of Ta. For a different value of Tg

Fig 2 represents the variation of the COP as a function of Ta for different values of Tg. It has been observed that the coefficient of performance decreases with the increase in the temperature of the absorber Ta. This fact is due to the circulation rate which increases with the increase in the concentration of rich refrigerant in the absorber.

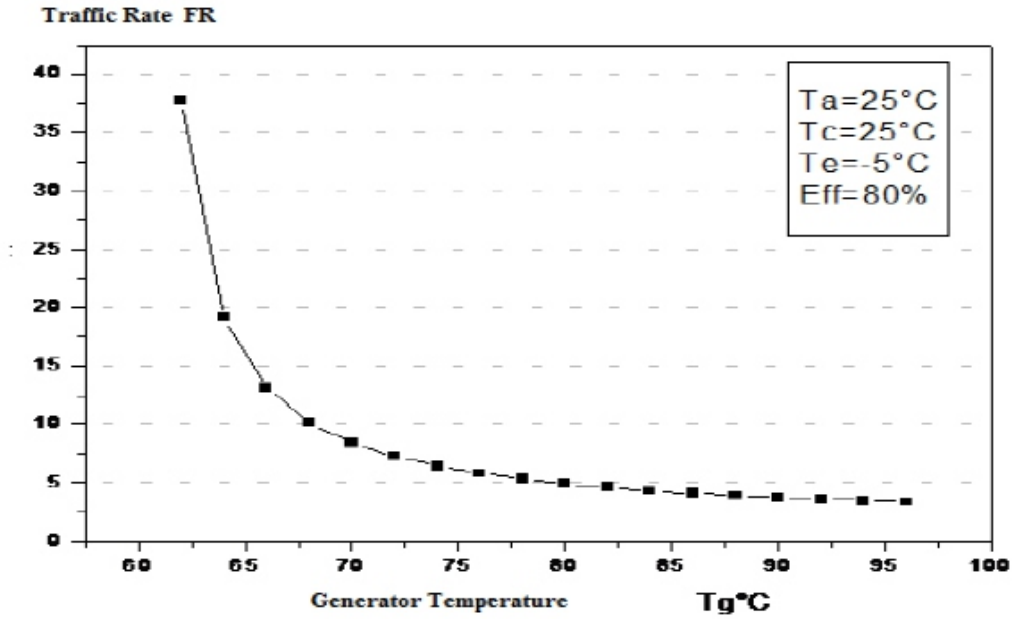

Fig.3: variation of FR as a function of Tg

Fig.3 shows the influence of the increase in Tg on the rate of circulation. We note that the increase in Tg allows the reduction of the rate of circulation FR, for Tg temperature values below 80 ° C. This decrease can be explained by increasing the concentrated solution by increasing Tg, which allows the increase in the degassing range (ΔX) and therefore the decrease in FR.

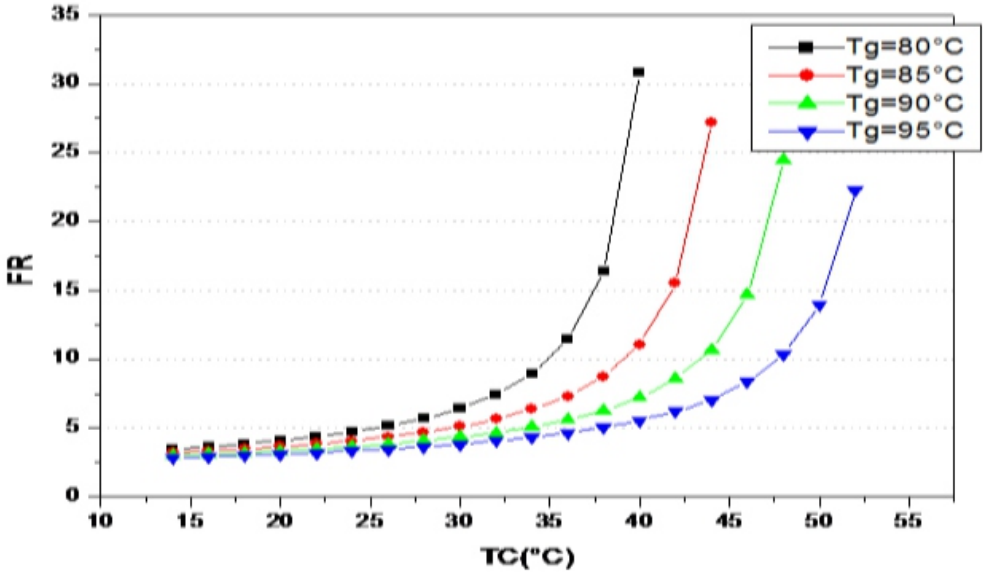

Fig.4: variation of FR as a function of Tc. For a different value of Tg

Fig.4 shows the variation of the FR as a function of Tc. For Tg <85 ° C, we note the large increase in RF with increasing Tc, while increasing Tg note that the rate of RF circulation decreases. This decrease in RF can be explained by the reduction of concentrated solution Xc following the increase in pressure data and critical details.

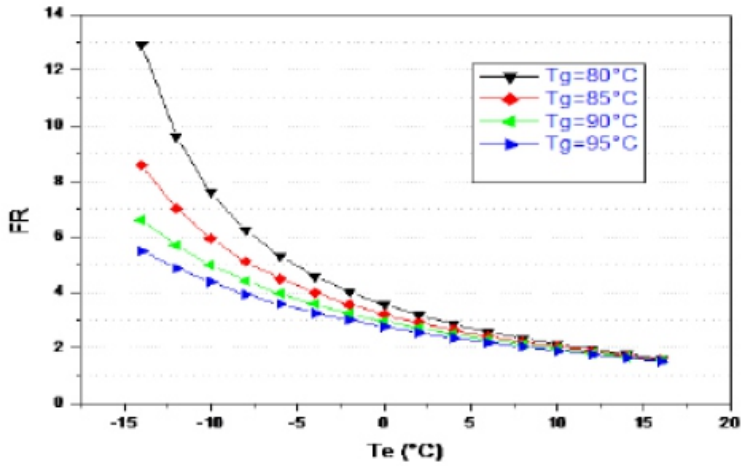

Fig.5: variation of FR as a function of Te, for different values of Tg

Fig.5: is presented the variation of the circulation rate as a function of the evaporator temperature FR = f (Te). The results show the significant decrease in RF with increasing Te for low values of generator temperature (Tg <85 ° C). This is probably explained by the fact that increasing Te increases the value of dilute solution Xd, and therefore decreases FR

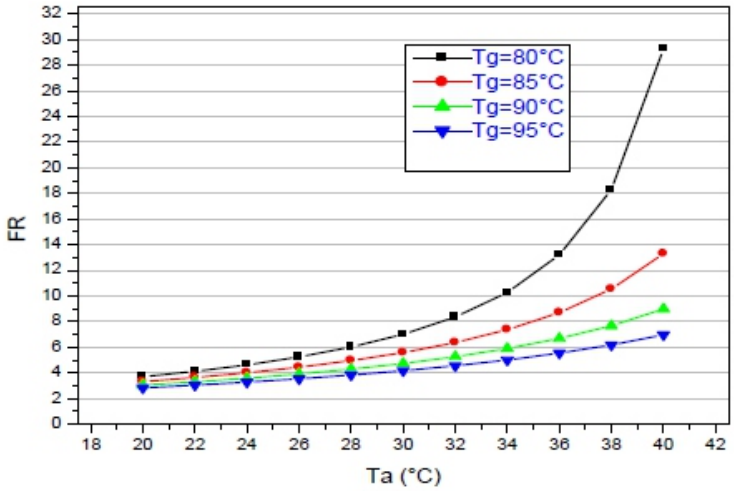

Fig.6: variation of FR as a function of Ta, for different values of Tg

Fig.6: represents the variation of the FR as a function of Ta, for different values of Tg. For values of Ta> 30 ° C, we notice the significant increase in the circulation rate, while increasing Tg> 85 ° C we see the decrease in the circulation rate (FR). This can be explained by the decrease in the diluted solution Xd following the increase in Ta.

V. CONCLUSION

The use of solar energy in sunny countries is an effective way to compensate for the lack of energy especially in rural areas where it is sometimes difficult and expensive to supply them with the electricity grid. Also, Algeria is a country in which there is strong solar radiation in several regions. It is important to exploit this natural resource in the field of cold production, especially in the absorption machine for air conditioning because of its simplicity of design. Among these possibilities, the absorption solar air conditioning technique is the most commonly used. It represents more than 82% of solar air conditioning technologies used. The most common technique is to use solar collectors to provide heat which is

directed to an absorption machine. The results show a decrease in the coefficient of performance of the machine COP which accompanies the increase in the temperature of the condenser Tc The results showed an increase in the COP associated with the increase in the evaporator temperature Te and the generator temperature Tg.

REFERENCE

[1] T Nunez., W Mittelbach ., H-M Henning. Développent of an adsorption chiller and heat pump for domestic heating and air-conditioning applications, Applied Thermal Engineering, 2007.

[2] Benaoudia, M. 2001. Les contributions à l'optimisation en régime stationnaire des installations frigorifiques à absorption avec la solution Hydro- Ammoniacale, thèse de Doctorat, Université Technique de Construction BUCAREST.

[3] A. C. Alihonou, C. T. Guidi, M. L. Vissoh, A. Adjagodo, E. A. Sanya, and M. A. Djikpo Tchibozo, "Climatisation solaire à absorption, mode de fonctionnement et description des différents éléments d'une unité de climatisation solaire dans le monde : Revue de littérature," Int. J. Biol. Chem. Sci., vol. 13, no. 3, p. 1890, 2019, doi: 10.4314/ijbcs.v13i3.55.

[4] Khalid, A, Joudi, Ali.H. Lafta. 2001, Simulation of a simple absorption refrigeration system, Energy Conversion and Management, 42, 13, pp. 1575-1605.

[5] Kherris, S, M. Makhlouf, Dj. Zebbar et O. Sebbane. 2013, Contribution Study Of The Thermodynamics Properties Of The Ammonia-Water Mixtures, Thermal science, doi:10.2298/TSCI110206083K, 3, pp. 891–902.

[6] Armas, J.C., Lapido, M., Gomez, J.R., Valdivia, Y., 2011, A thermodynamic evaluation of chilled water central air conditioning systems using artificial intelligence tools. Ing. Investig. 31, 134_142.

[7] H.R. Lee, K.K. Koo, S. Jeong, J.S. Kim, H. Leec, Y.S. Oh, D.R. Park, Y.-S. Baek, Thermodynamic design data and performance evaluation of the water + lithium bromide + lithium iodide + lithium nitrate + lithium chloride system for absorption chiller, Applied Thermal Engineering, 20, 707-720, 2000.

Instructions for Authors

Essentials for Publishing in this Journal

1 Submitted articles should not have been previously published or be currently under consideration for publication elsewhere.

2 Conference papers may only be submitted if the paper has been completely re-written (taken to mean more than 50%) and the author has cleared any necessary permission with the copyright owner if it has been previously copyrighted.

3 All our articles are refereed through a double-blind process.

4 All authors must declare they have read and agreed to the content of the submitted article and must sign a declaration correspond to the originality of the article.

Submission Process

All articles for this journal must be submitted using our online submissions system. http://enrichedpub.com/ . Please use the Submit Your Article link in the Author Service area.

Manuscript Guidelines

The instructions to authors about the article preparation for publication in the Manuscripts are submitted online, through the e-Ur (Electronic editing) system, developed by **Enriched Publications Pvt. Ltd**. The article should contain the abstract with keywords, introduction, body, conclusion, references and the summary in English language (without heading and subheading enumeration). The article length should not exceed 16 pages of A4 paper format.

Title

The title should be informative. It is in both Journal's and author's best interest to use terms suitable. For indexing and word search. If there are no such terms in the title, the author is strongly advised to add a subtitle. The title should be given in English as well. The titles precede the abstract and the summary in an appropriate language.

Letterhead Title

The letterhead title is given at a top of each page for easier identification of article copies in an Electronic form in particular. It contains the author's surname and first name initial .article title, journal title and collation (year, volume, and issue, first and last page). The journal and article titles can be given in a shortened form.

Author's Name

Full name(s) of author(s) should be used. It is advisable to give the middle initial. Names are given in their original form.

Contact Details

The postal address or the e-mail address of the author (usually of the first one if there are more Authors) is given in the footnote at the bottom of the first page.

Type of Articles

Classification of articles is a duty of the editorial staff and is of special importance. Referees and the members of the editorial staff, or section editors, can propose a category, but the editor-in-chief has the sole responsibility for their classification. Journal articles are classified as follows:

Scientific articles:

1. Original scientific paper (giving the previously unpublished results of the author's own research based on management methods).

2. Survey paper (giving an original, detailed and critical view of a research problem or an area to which the author has made a contribution visible through his self-citation);

3. Short or preliminary communication (original management paper of full format but of a smaller extent or of a preliminary character);

4. Scientific critique or forum (discussion on a particular scientific topic, based exclusively on management argumentation) and commentaries. Exceptionally, in particular areas, a scientific paper in the Journal can be in a form of a monograph or a critical edition of scientific data (historical, archival, lexicographic, bibliographic, data survey, etc.) which were unknown or hardly accessible for scientific research.

Professional articles:

1. Professional paper (contribution offering experience useful for improvement of professional practice but not necessarily based on scientific methods);
2. Informative contribution (editorial, commentary, etc.);
3. Review (of a book, software, case study, scientific event, etc.)

Language

The article should be in English. The grammar and style of the article should be of good quality. The systematized text should be without abbreviations (except standard ones). All measurements must be in SI units. The sequence of formulae is denoted in Arabic numerals in parentheses on the right-hand side.

Abstract and Summary

An abstract is a concise informative presentation of the article content for fast and accurate Evaluation of its relevance. It is both in the Editorial Office's and the author's best interest for an abstract to contain terms often used for indexing and article search. The abstract describes the purpose of the study and the methods, outlines the findings and state the conclusions. A 100- to 250-Word abstract should be placed between the title and the keywords with the body text to follow. Besides an abstract are advised to have a summary in English, at the end of the article, after the Reference list. The summary should be structured and long up to 1/10 of the article length (it is more extensive than the abstract).

Keywords

Keywords are terms or phrases showing adequately the article content for indexing and search purposes. They should be allocated heaving in mind widely accepted international sources (index, dictionary or thesaurus), such as the Web of Science keyword list for science in general. The higher their usage frequency is the better. Up to 10 keywords immediately follow the abstract and the summary, in respective languages.

Acknowledgements

The name and the number of the project or programmed within which the article was realized is given in a separate note at the bottom of the first page together with the name of the institution which financially supported the project or programmed.

Tables and Illustrations

All the captions should be in the original language as well as in English, together with the texts in illustrations if possible. Tables are typed in the same style as the text and are denoted by numerals at the top. Photographs and drawings, placed appropriately in the text, should be clear, precise and suitable for reproduction. Drawings should be created in Word or Corel.

Citation in the Text

Citation in the text must be uniform. When citing references in the text, use the reference number set in square brackets from the Reference list at the end of the article.

Footnotes

Footnotes are given at the bottom of the page with the text they refer to. They can contain less relevant details, additional explanations or used sources (e.g. scientific material, manuals). They cannot replace the cited literature.
The article should be accompanied with a cover letter with the information about the author(s): surname, middle initial, first name, and citizen personal number, rank, title, e-mail address, and affiliation address, home address including municipality, phone number in the office and at home (or a mobile phone number). The cover letter should state the type of the article and tell which illustrations are original and which are not.

Address of the Editorial Office:

Enriched Publications Pvt. Ltd.
S-9,IInd FLOOR, MLU POCKET,
MANISH ABHINAV PLAZA-II, ABOVE FEDERAL BANK,
PLOT NO-5, SECTOR -5, DWARKA, NEW DELHI, INDIA-110075,
PHONE: - + (91)-(11)-45525005

Note